ORGANOMETALLICS

pubs.acs.org/Organometallics Article

Functionalization of Rh^{III}–Me Bonds: Use of "Capping Arene" Ligands to Facilitate Me–X Reductive Elimination

Shunyan Gu,[#] Junqi Chen,[#] Charles B. Musgrave III, Zoë M. Gehman, Laurel G. Habgood, Xiaofan Jia, Diane A. Dickie, William A. Goddard III,* and T. Brent Gunnoe*

Cite This: *Organometallics* 2021, 40, 1889–1906 Read Online

ABSTRACT: We show how to improve the yield of MeX from CH_4 activation catalysts from 12% to 90% through the use of "capping arene" ligands. Four $(FP)Rh^{III}(Me)(TFA)_2$ {FP = "capping arene" ligands, including 8,8′-(1,2-phenylene)diquinoline (6-FP), 8,8′-(1,2-naphthalene)diquinoline (6-^{NP}FP), 1,2-bis(*N*-7-azaindolyl)benzene (5-FP), and 1,2-bis(*N*-7-azaindolyl)naphthalene (5-^{NP}FP)} complexes. These complexes and $(dpe)Rh^{III}(Me)(TFA)_2$ (dpe = 1,2-di-2-pyridylethane) were synthesized and tested for their performance in reductive elimination of MeX (X = TFA or halide). The FP ligands were used with the goal of blocking a coordination site to destabilize the Rh^{III} complexes and facilitate MeX reductive elimination. On the basis of single-crystal X-ray diffraction studies, the 6-FP and 6-^{NP}FP ligated Rh complexes have Rh–arene distances shorter than those of the 5-FP and 5-^{NP}FP Rh complexes; thus, it is expected that the Rh–arene interactions are weaker for the 5-FP complexes than for the 6-FP complexes. Consistent with our hypothesis, the 5-FP and 5-^{NP}FP Rh^{III} complexes demonstrate improved performance (from 12% to ∼60% yield) in the reductive elimination of MeX. The reductive elimination of MeX from $(FP)Rh^{III}(Me)(TFA)_2$ can be further improved by the use of chemical oxidants. For example, the addition of 2 equiv of AgOTf leads to 87(2)% yield of MeTFA and can be achieved in CD_3CN at 90 °C using $(5\text{-FP})Rh(Me)(TFA)_2$.

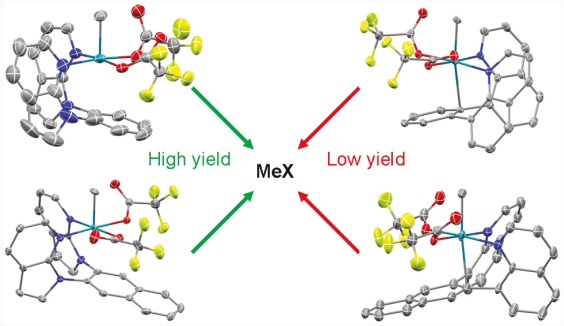

INTRODUCTION

The partial oxidation of alkanes into alcohols and other oxygenates has been of interest due to the potential to develop more efficient processes for alkane upgrading.[1−9] However, the inertness of alkanes and the fact that their partially oxidized products are often more reactive than alkane substrates make selective alkane partial oxidation a substantial challenge.[4,5,10−13] Since Shilov and co-workers' discovery of platinum-catalyzed alkane functionalization,[4,14,15] electrophilic metal complexes have been studied for C–H activation and functionalization.[16−24] The Catalytica process, reported by Periana and co-workers in 1998, demonstrates an example of converting methane to a methanol derivative with high selectivity using $(bpym)PtCl_2$ (bpym = 2,2′-bipyrimidinyl) as the catalyst.[21] In this process, the Pt^{II} catalyst has been proposed to activate the C–H bond of the alkane, followed by oxidation to Pt^{IV}, and then reductive elimination of MeX to give the functionalized product and regenerate the Pt^{II} catalyst.[4,15,21,25] Thus, a net two-electron reductive elimination of MeX is a key step in the catalytic cycle. However, oleum, a super acidic medium, is required to achieve reasonable reaction rates due to the inhibition of catalysis as a result of solvent coordination.

The coordination of solvents to electrophilic Pt^{II} is a limitation of the Shilov type catalytic alkane functionalization. On the basis of periodic trends, it might be anticipated that Rh^{I} or Ir^{I} complexes might be less electrophilic than Pt^{II}, hence providing a potential alternative to the Pt-based Shilov-type chemistry.[26,27] In a Rh analog of Pt-based Shilov catalysis, C–H activation of alkanes by Rh^{I} and reductive elimination of MeX (X = halide or pseudo halide) from X–Rh^{III}–Me would be key steps (Scheme 1). Despite some reports of Rh-catalyzed methane oxidation using molecular catalysts,[18] reductive elimination of MeX (or, more broadly, RX where R = alkyl) is often a challenge due to unfavorable thermodynamics of $Rh^{III} \rightarrow Rh^{I}$ redox reactions.[7,8,28−33] For Rh catalysis, C–H activation at the Rh^{I} or Rh^{III} oxidation state is also possible,[34,35] but for alkane activation, C–H bond breaking by Rh^{I} seemingly has more precedent.[33,36−39] With our recent work on Rh-mediated C–H activation and

Received: April 8, 2021
Published: May 3, 2021

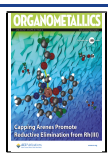

https://doi.org/10.1021/acs.organomet.1c00223
Organometallics 2021, 40, 1889–1906

Scheme 1. Possible Mechanism for Rh-Catalyzed Alkane Functionalization That Is Analogous to Some Pt-Catalyzed Reactions

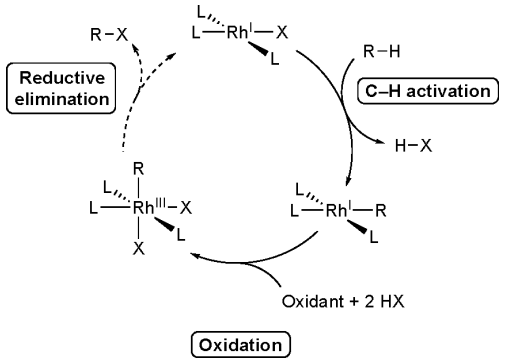

Scheme 2. Design of Capping Arene Ligands Including 5-^{X}FP and 6-^{X}FP Ligands Discussed in This Work

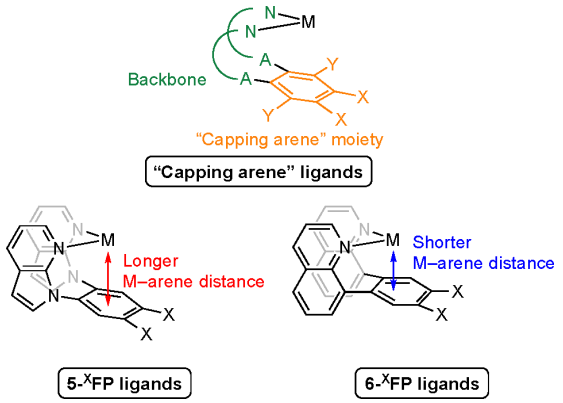

functionalization, it has been of interest to understand how ligand modification affects thermodynamics and kinetics of redox processes involving Rh^{I}, Rh^{II}, Rh^{III}, and Rh^{IV} species.[31,40−49]

Some recent reports have focused on the reductive elimination reactions from Rh^{III} complexes.[48,50−56] One strategy to facilitate reductive elimination is to use steric bulk to destabilize Rh^{III} species and render Rh^{I} species more thermodynamically favorable. The Milstein group reported mechanistic studies focusing on this strategy for the reductive elimination of MeX (X = halide) from pincer ligated Rh^{III} complexes.[50−52] Recently, we expanded studies of (^{R}PNP)Rh complexes to include both alkyl and aryl substituents on the PNP ligand and found a trend based on phosphine substituent size: Larger ligands promote reductive elimination from Rh^{III}.[48] A second strategy to shift the Rh^{I}/Rh^{III} redox couple toward Rh^{I} is to tune the electronic properties of the ligand. For example, our group studied the reductive elimination of MeX from (^{X}terpy)Rh(Me)(Cl)(I) complexes (^{X}terpy = 4,4′,4″-tri-*tert*-butylpyridine or 4,4′,4″-trinitroterpyridine) where the electron-withdrawing nitro group facilitates the formation of MeX compared to the *tert*-butyl substituents on the terpy ligand.[53,54] In addition, chemical oxidants have been shown to facilitate reductive elimination reactions by placing the metal in a higher oxidation state, thus favoring a subsequent reductive elimination reaction.[57,58]

Previously, our group reported a series of Rh complexes with "capping arene" ligands where a coordination site of the Rh center is blocked by the arene moiety (Scheme 2, top).[44,59−61] In this series of ligands, including 5-^{X}FP and 6-^{X}FP ligands (see Scheme 2 for explanation of abbreviations), the distance between the metal center and the capping arene can be tuned by adjusting the N−A backbone (see Scheme 2). Also, the properties of the arene moiety can be modified using different X and Y substituents. In general, we anticipate metal-arene bonding interactions, if present, to be weak. Compared with 6-^{X}FP ligands, 5-^{X}FP ligands enforce longer M−arene distances and, presumably, weaker ligand-to-metal electron donation (Scheme 2, bottom). We considered using capping arene ligands as a strategy to facilitate reductive elimination of MeX from Rh^{III} complexes since the capping arene ligand can potentially prevent the formation of electronically saturated 18-electron Rh^{III} complexes, thus destabilizing the Rh^{III} complexes relative to the Rh^{I} complexes that would result from reductive elimination processes. In this work, we synthesized a series of capping arene pro-ligands (FP) and corresponding (FP)Rh^{III}(Me)$(TFA)_2$ complexes. On the basis of the metal−arene distances and the anticipated changes in bond strengths (see above), we expected that MeTFA elimination from 5-FP ligands would be more readily facilitated relative to that from 6-FP ligands and that FP-ligated Rh complexes might have an advantage for MeTFA reductive elimination over related complexes with more classic octahedral coordination and 18-electron counts. Herein, we demonstrate that the success of MeX reductive elimination is dependent on the use of 5-^{X}FP ligands and that the incorporation of oxidants, such as Ag^{I}, leads to yields of MeX up to 87(2)%.

RESULTS AND DISCUSSION

Synthesis and Characterization of Ligands and Rh^{III}−Me Complexes. The use of *N*-7-azaindolyl and quinoline-based ligands allow for the control of distances between the Rh metal center and the arene due to the different bond angles in six-membered and five-membered rings (Scheme 2).[62] This provides a strategy to evaluate the impact of the Rh−arene distance on reductive functionalization of Rh^{III}−Me groups. We selected four capping arene ligands, 5-FP (1,2-bis(*N*-7-azaindolyl)benzene, complexes labeled with **1**), 6-FP (8,8′-(1,2-phenylene)diquinoline, complexes labeled with **2**), 5-^{NP}FP (2,3-bis(*N*-7-azaindolyl)naphthalene, complexes labeled with **3**), and 6-^{NP}FP (8,8′-(2,3-naphthalene)diquinoline, complexes labeled with **4**). The ^{NP} designation indicates that the arene group is a naphthyl moiety. Also, we chose a non-capping arene ligand (dpe, 1,2-di-2-pyridylethane, complexes labeled with **5**) to compare the formation of Me−X for Rh^{III} complexes with a similar bis-pyridyl ligand motif that lacks the capping arene feature.[63,64] The pro-ligand 6-FP (**2**) was synthesized by a palladium-catalyzed Suzuki coupling reaction using 8-quinolylboronic acid and 1,2-diiodobenzene as the starting materials (Scheme 3), and 6-^{NP}FP (**4**) was synthesized using a similar method but with Cs_2CO_3 as the base and without the use of water.[59,62] Most peaks in the ^{1}H NMR spectrum of 6-FP are broadened (Figure S7), which is likely due to the hindered rotation of the C−C bond connecting the arene and quinoline moieties. The compound 5-^{NP}FP (**3**) was synthesized using a procedure similar to that used for 5-FP.[63]

https://doi.org/10.1021/acs.organomet.1c00223
Organometallics 2021, 40, 1889−1906

Scheme 3. Synthesis of 6-FP (8,8′-(1,2-Phenylene)diquinoline, 2), 5-^{NP}FP (2,3-Bis(*N*-7-azaindolyl)naphthalene, 3), and 6-^{NP}FP (8,8′-(2,3-Naphthalene)diquinoline, 4)

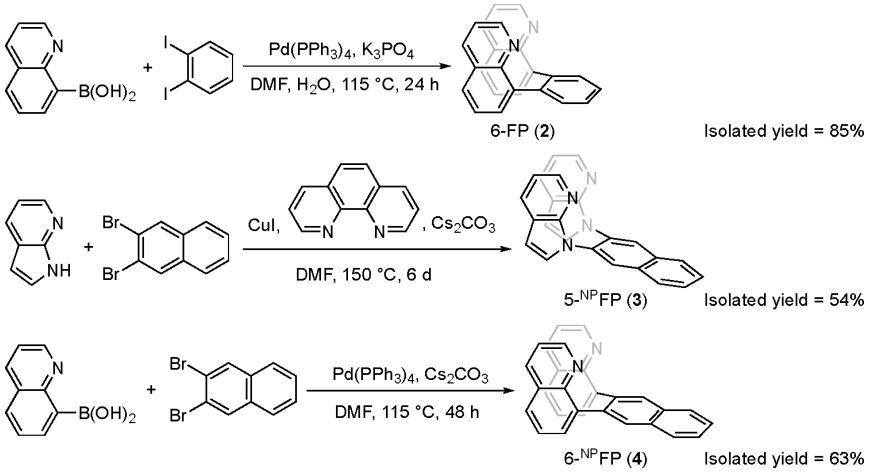

Scheme 4. Synthetic Routes to (5-FP)Rh(Me)(TFA)$_2$ (1c, Top) and (dpe)Rh(Me)(TFA)$_2$ (5c, Bottom)[a]

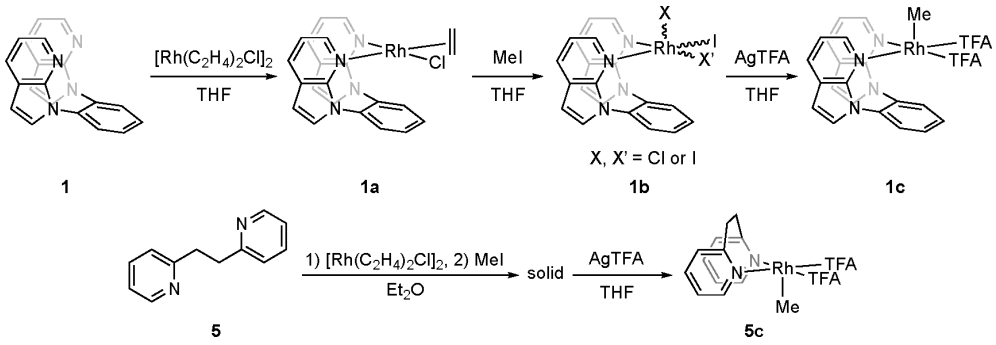

[a]The procedures for **2a**, **3a**, and **4a** are similar to that of **1c**.

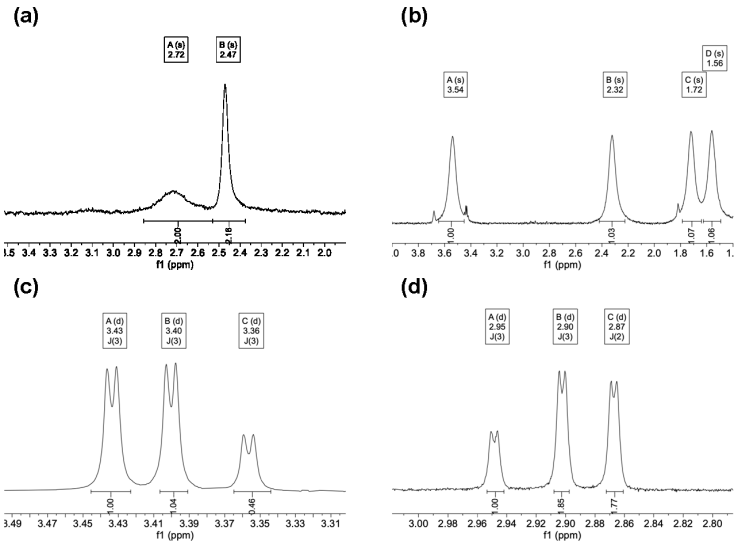

Figure 1. Selected sections of ^{1}H NMR spectra of **1a**, **2a**, **1b**, and **2b**. (a) Coordinated ethylene peaks of (5-FP)Rh(Cl)(η^2-C_2H_4) (**1a**). (b) Coordinated ethylene peaks of (6-FP)Rh(Cl)(η^2-C_2H_4) (**2a**). (c) Methyl peaks of (5-FP)Rh(Me)(X)(X′) (**1b**). (d) Methyl peaks of (6-FP)Rh(Me)(X)(X′) (**2b**) (X and X′ = Cl or I).

https://doi.org/10.1021/acs.organomet.1c00223
Organometallics 2021, 40, 1889−1906

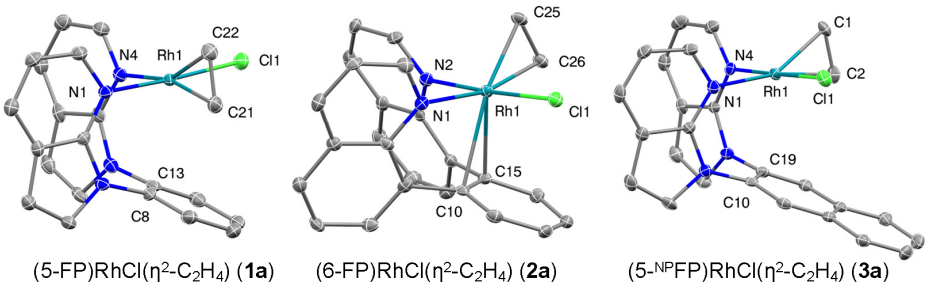

Figure 2. ORTEPs of (5-FP)Rh(Cl)(η^2-C_2H_4) (**1a**), (6-FP)Rh(Cl)(η^2-C_2H_4) (**2a**), and (5-^{NP}FP)Rh(Cl)(η^2-C_2H_4) (**3a**). Ellipsoids are drawn at the 50% probability level, and hydrogen atoms and noncoordinating solvent are omitted for clarity.

Rh^{III} methyl complexes were synthesized as shown in Scheme 4. The Rh precursor, $[Rh(\eta^2\text{-}C_2H_4)_2(\mu\text{-}Cl)]_2$, reacts with compound **1** in THF to generate (5-FP)Rh(Cl)(η^2-C_2H_4) (**1a**). The complexes (6-FP)Rh(Cl)(η^2-C_2H_4) (**2a**), (5-^{NP}FP)Rh(Cl)(η^2-C_2H_4) (**3a**), and (6-^{NP}FP)Rh(Cl)(η^2-C_2H_4) (**4a**) were synthesized using the same method. The ^{1}H NMR spectra of **1a** and **2a** (Figure 1, top) indicate asymmetric complexes, and the coordinated ethylene peaks of **1a** appear as two broad peaks with an integration of two protons each. Single-crystal X-ray diffraction studies elucidated the solid-state structures of complexes **1a**, **2a**, and **3a** (Figure 2). These data confirm rapid rotation of the coordinated ethylene in **1a** on the time scale of the ^{1}H NMR experiment. In contrast, the resonances due to coordinated ethylene for **2a** appear as four broad peaks with an integration of one proton each. This is an indication of the activation barrier for ethylene in **1a** being lower than that in **2a**. The crystal structures of **1a** and **2a** are consistent with the proposed differences in activation barriers for ethylene rotation as the distances between Rh and the two nearest arene carbon atoms for **2a** (2.578(3) and 2.553(3) Å) are closer than those for **1a** (3.110(3) and 3.041(3) Å) (Figure 2, Table 1), which we propose leads to steric inhibition of olefin rotation for **2a**. Consistent with observations by ^{1}H NMR, in ^{13}C{^{1}H} NMR spectra of **1a** and **2a** (Figures S2 and S12), there is one broad peak for the coordinated ethylene of **1a** and two peaks for complex **2a**. A small coupling constant (<2 Hz) is observed by ^{1}H NMR spectroscopy between Rh and the H atoms of the capping arene of **2a**, indicating η^2-coordination between the Rh center and the arene ring. Similar observations were made for **3a** and **4a**. In **4a**, the two carbon atoms coordinating to Rh appear as a singlet and a doublet with $^1J_{RhC}$ of 6 Hz in the ^{13}C{^{1}H} NMR spectrum. They were determined, by HSQC spectroscopy (Figure S37), to be the 1,2-carbon of the naphthalene ring, which is different from the position of η^2-interaction in **2a** (Scheme 5).

Table 1. Selected Bond Lengths for (5-FP)Rh(Cl)(η^2-C_2H_4) (1a), (6-FP)Rh(Cl)(η^2-C_2H_4) (2a), and (5-^{NP}FP)Rh(Cl)(η^2-C_2H_4) (3a) Based on Single-Crystal X-ray Structures

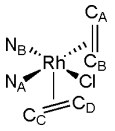

bond[a]	bond length (Å)		
	1a	2a	3a
Rh−N_A	2.1261(19)	2.200(3)	2.130(2)
Rh−N_B	2.0323(19)	2.031(3)	2.035(3)
Rh−Cl	2.3531(6)	2.3549(8)	2.3392(9)
Rh−C_A	2.109(2)	2.081(3)	2.094(3)
Rh−C_B	2.103(2)	2.081(3)	2.112(3)
Rh−C_C	3.110(3)	2.578(3)	3.118(3)
Rh−C_D	3.041(3)	2.553(3)	3.013(3)

[a]N_A refers to the N atom *trans* to ethylene ligand. C_A refers to the carbon further from the capping arene moiety. C_C refers to the carbon on the capping arene moiety bonding with the backbone and closer to N_A.

Scheme 5. η^2-*C*,*C* Interactions (Red Dashed Lines) between the Rh Center and Arene Moiety in 2a and 4a[a]

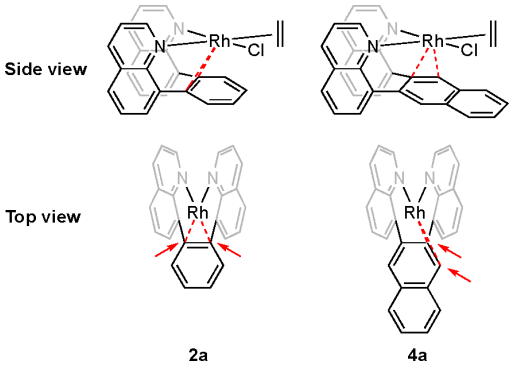

[a]The carbons interacting with Rh are labeled with red arrows in the top view of the complexes.

Reacting complexes **1a**, **2a**, **3a**, and **4a** with MeI in THF results in the formation of the Rh^{III}−Me complexes (5-FP)Rh(Me)(X)(X′) (**1b**), (6-FP)Rh(Me)(X)(X′) (**2b**), (5-^{NP}FP)Rh(Me)(X)(X′) (**3b**), and (6-^{NP}FP)Rh(Me)(X)(X′) (**4b**) (X and X′ = Cl or I). There could be isomers of oxidative addition product, (FP)Rh(Me)(Cl)(I), or (FP)Rh-(Me)$(Y)_2$ (Y = Cl or I). A total of three species are formed, which is indicated by the results observed in the ^{1}H NMR spectra of **1b**, **2b**, and **3b** (Figures 1c,d and Figures S25 and S38). In the ^{1}H NMR spectra of **1b** and **2b**, three resonances for the Rh−CH_3 ligands, each with a $^2J_{RhH}$ of 2−3 Hz, can be observed. In the ^{1}H NMR spectrum of **4b**, there are as many as seven methyl resonances, which we have not delineated.

Next, 2 equiv of AgTFA (TFA = trifluoroacetate) were used to replace the chloride and iodide ligands of **1b**, **2b**, **3b**, and

https://doi.org/10.1021/acs.organomet.1c00223
Organometallics 2021, 40, 1889−1906

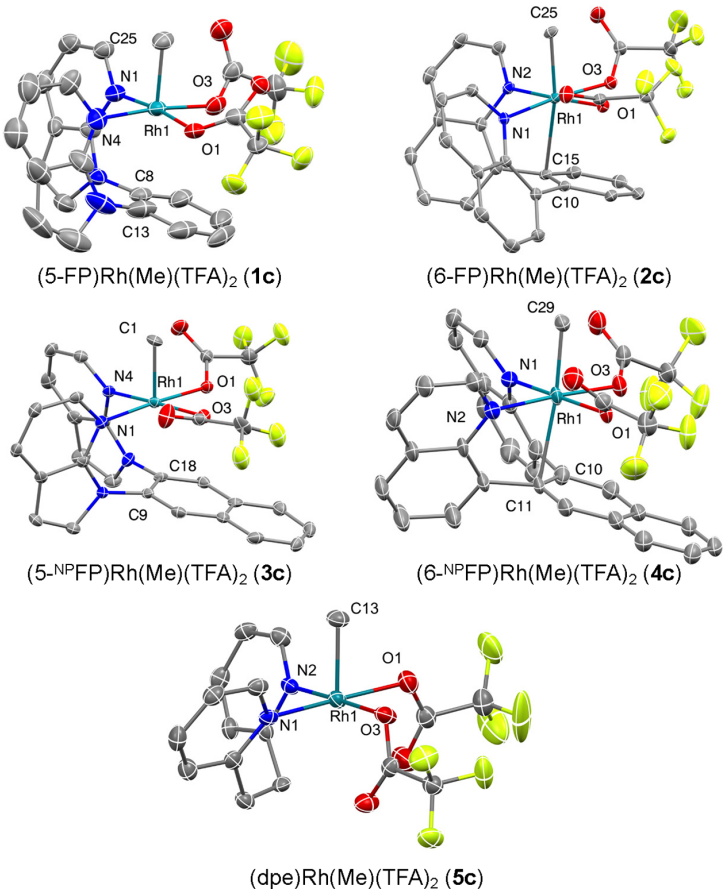

Figure 3. ORTEPs of (5-FP)Rh(Me)$(TFA)_2$ (**1c**), (6-FP)Rh(Me)$(TFA)_2$ (**2c**), (5-^{NP}FP)Rh(Me)$(TFA)_2$ (**3c**), (6-^{NP}FP)Rh(Me)$(TFA)_2$ (**4c**), and (dpe)Rh(Me)$(TFA)_2$ (**5c**). Ellipsoids are drawn at the 50% probability level. Hydrogen atoms and noncoordinating solvent are omitted for clarity. For **1c**, only one of the three chemically equivalent but crystallographically distinct molecules in the asymmetric unit is shown.

Table 2. Selected Bond Lengths for (5-FP)Rh(Me)$(TFA)_2$ (1c), (6-FP)Rh(Me)$(TFA)_2$ (2c), (5-^{NP}FP)Rh(Me)$(TFA)_2$ (3c), (6-^{NP}FP)Rh(Me)$(TFA)_2$ (4c), and (dpe)Rh(Me)$(TFA)_2$ (5c)

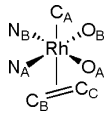

	bond length (Å)				
bond[a]	1c	2c	3c	4c	5c
Rh–N_A	2.040(10)	2.0384(15)	2.043(3)	2.047(4)	2.015(4)
Rh–N_B	2.038(9)	2.0567(15)	2.046(3)	2.064(5)	2.048(4)
Rh–O_B	2.014(7)	2.0321(13)	2.043(3)	2.053(3)	2.047(4)
Rh–O_A	2.045(7)	2.0458(12)	2.045(3)	2.055(4)	2.066(3)
Rh–C_A	2.043(9)	2.0747(18)	2.028(4)	2.049(4)	2.024(5)
Rh–C_B	2.749(10)	2.6309(18)	2.791(3)	2.529(4)	N/A
Rh–C_C	2.878(11)	2.5722(18)	2.847(4)	2.826(5)	N/A

[a]N_A and N_B are *trans* to O_B and O_A respectively. C_B and C_C refer to the carbons of the capping arene that are bonding with the ligand backbone. For **1c**, the table lists only one of the three chemically equivalent but crystallographically distinct molecules in the asymmetric unit.

4b with TFA to give the products (5-FP)Rh(Me)$(TFA)_2$ (**1c**), (6-FP)Rh(Me)$(TFA)_2$ (**2c**), (5-^{NP}FP)Rh(Me)$(TFA)_2$ (**3c**), and (6-^{NP}FP)Rh(Me)$(TFA)_2$ (**4c**). The ^{1}H NMR spectra of **1c** and **2c** demonstrate a single species with mirror symmetry, which indicates that the methyl ligands are *trans* to the capping arene group. The crystal structures of **1c** and **2c** are consistent with the characterizations based on NMR data (Figure 3). Resonances due to the methyl ligands are observed at 3.82 and 3.27 ppm for **1c** and **2c** in CD_2Cl_2, both appearing as doublets with $^2J_{RhH}$ of 2 Hz. In the crystal

https://doi.org/10.1021/acs.organomet.1c00223
Organometallics 2021, 40, 1889−1906

structure of **2c**, the quinoline moiety is distorted to better fit an octahedral structure of Rh^{III} complex. The arene ring of **2c** is positioned with Rh−C10 and Rh−C15 distances of 2.631(2) Å and 2.572(3) Å, respectively (Table 2). These are longer than typical Rh−C bonds, but these are sufficiently close to consider weak η^2-coordination, which is supported by the longer C10−C15 distance (1.415(3) Å) in the arene moiety.[63−70]

We synthesized (dpe)Rh(Me)$(TFA)_2$ (**5c**) as a comparison to capping arene complexes **1c**−**4c**. The dpe ligand was mixed with $[Rh(\eta^2\text{-}C_2H_4)_2(\mu\text{-}Cl)]_2$ in diethyl ether, and MeI was added to make the Rh^{III} complex. The resulting solid was suspended in THF, and AgTFA was used to abstract the chloride and iodide and give the product of (dpe)Rh(Me)-$(TFA)_2$ (**5c**). In the ^1H NMR spectrum, there are four resonances due to pyridyl protons, indicating the presence of mirror symmetry. The methyl peak appears as a doublet at 3.44 ppm with $^2J_{RhH}$ = 3 Hz in CD_2Cl_2. The crystal structure of **5c** (Figure 3, bottom) is consistent with the NMR data. When dissolving the complex in CD_3CN, new species were observed in the ^1H NMR spectrum, which indicates likely coordination of CD_3CN.

Reductive Elimination of MeX from (L)Rh(Me)$(TFA)_2$ (L = Capping Arene Ligand or dpe) in CD_3CN. Studies of the reductive functionalization of Rh^{III}−Me bonds to form MeX from **1c** and **2c** were performed using ^1H NMR spectroscopy with 0.01 M solutions of the Rh complex. Solvent screening experiments of eight different solvents were performed to select the optimal condition (Table S1). In C_6D_6, THF-d_8, and DMSO-d_6, MeX formation was not observed at temperatures up to 120 °C. The highest yield, 59(1)% (in this report, standard deviations are the result of a minimum of three independent experiments), was achieved using CD_3CN as the solvent at 90 °C after 48 h of reaction (Scheme 6 and Table S1).

Scheme 6. Reductive Elimination of MeTFA from (5-FP)Rh(Me)$(TFA)_2$ (1c)

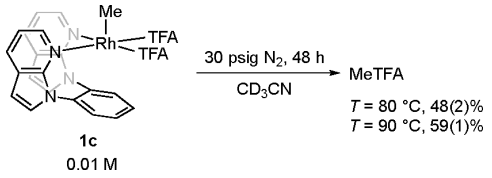

Dissolving **1c** and **2c** in CD_3CN at room temperature results in a color change from yellow to pale yellow over approximately 24 h (Figure S52), indicating the likely formation of new species. ^1H NMR and ^{19}F NMR spectra after 24 h in CD_3CN indicate that an equilibrium was established. The process was accelerated at 90 °C, and equilibrium was reached in 15 min. The ratio of the newly formed complex and **1c** is determined to be ∼ 2:1 by ^1H NMR integration. For the reaction of **1c**, a set of new resonances is observed in the aromatic region of the ^1H NMR spectrum that is consistent with formation of an asymmetric complex. A new resonance due to Rh−CH_3 peak is observed at 3.64 ppm, and a new peak in the ^{19}F NMR spectrum is found upfield compared to **1c** (Figures 4a and 4b). Also, in the ^{19}F NMR spectrum a broad peak is observed at −72.7 ppm. These observations are consistent with the dissociation of one TFA ligand and coordination of CD_3CN to form [(5-FP)Rh(Me)(TFA)(CD_3CN)][TFA] (**1ci**) (Scheme 7). Upon removal of solvent under vacuum, **1ci** converts back to **1c**, indicating that the coordinated acetonitrile ligand is likely labile. For **2c**, similar reactions were observed (Figures 4c and 4d). Notably, the formation of [(FP)Rh(Me)(TFA)-(CD_3CN)][TFA] (FP = 5-FP or 6-FP, **1ci** and **2ci**) occurs during *in situ* NMR studies of reductive functionalization (Figure 4). The formation of **1ci** and **2ci** might explain why MeX reductive functionalization achieves the highest yield in CD_3CN as there is precedent for acetonitrile facilitating reductive elimination.[51,52]

The performance of **1c**, **2c**, **3c**, **4c**, and **5c** in reductive elimination of MeTFA in CD_3CN was compared. Complexes **1c** and **3c** gave similar yields of MeTFA of 59(1)% and 49(1)% after 48 h (Table 3). However, **2c** and **4c** only gave only 5(0)% and 2(0)% yields of MeTFA after 144 and 48 h, and decomposition was observed in the ^1H NMR spectra. **5c** gave 12(1)% yield of MeTFA under the same conditions. These results are consistent with our hypothesis that weaker bonding in (5-FP)Rh^{III} complexes can facilitate reductive elimination, in this case the differences in the Rh−arene interaction of the FP ligands. For complexes **1c** and **3c**, the ligand structure positions the arene farther from Rh than the arene groups of **2c** and **4c**, as indicated by the solid-state X-ray structures (Figure 3 and Table 2). Thus, we speculate weaker arene/Rh bonding for **1c** and **3c** compared to that in **2c** and **4c**, which could destabilize the Rh^{III} complexes and facilitate reductive elimination of MeTFA. For **5c**, although it appears as five-coordinate complex in the crystal structure (Figure 3), immediate reaction was observed when dissolved in CD_3CN, indicating coordination of CD_3CN. The newly formed six-coordinate structure likely increases the energy barrier of reductive elimination.

To better understand the data displayed in Table 3, we performed density functional theory (DFT) calculations at the B3LYP-D3 level (see the "Computational Methods" section for details) to elucidate the mechanism for MeTFA formation from the Rh^{III}−Me precursors. We began with the equilibrium structures [(5-FP)Rh(Me)(TFA)(MeCN)](TFA) (**1ci**) and [(6-FP)Rh(Me)(TFA)(MeCN)](TFA) (**2ci**), in which a labile CH_3CN is coordinated to Rh. This leaves one of the two TFA ligands bound to the Rh center, while the second TFA is located in the first solvent shell, making several hydrogen bonds to the Rh complex (see the Supporting Information). As observed experimentally, the distances between the Rh and the carbons of the capping arene vary depending on the diimine ligand. For **1ci**, DFT predicts the Rh−C_C and Rh−C_B distances to be 2.89 and 2.95 Å. For **2ci**, the Rh−C_C and Rh−C_B distances are predicted to be 2.70 and 2.85 Å. Thus, we confirm experimental findings that the 6-FP ligand forces close proximity of the Rh with the capping arene carbons, while the 5-FP ligand allows the Rh and the capping arene to be farther apart.

We considered two likely pathways for MeTFA formation: (1) a unimolecular reaction in which the Rh undergoes C−O reductive elimination to afford MeTFA or (2) a bimolecular S_N2 reaction in which TFA in the first solvent shell attacks the methyl group to produce MeTFA (Scheme 8). DFT predicts the barriers for intramolecular reductive elimination to be substantially higher than the barriers for S_N2. For **1ci** with the 5-FP ligand, DFT predicts a reductive elimination barrier of 42.4 kcal/mol, while the S_N2 barrier is predicted to be more

https://doi.org/10.1021/acs.organomet.1c00223
Organometallics 2021, 40, 1889−1906

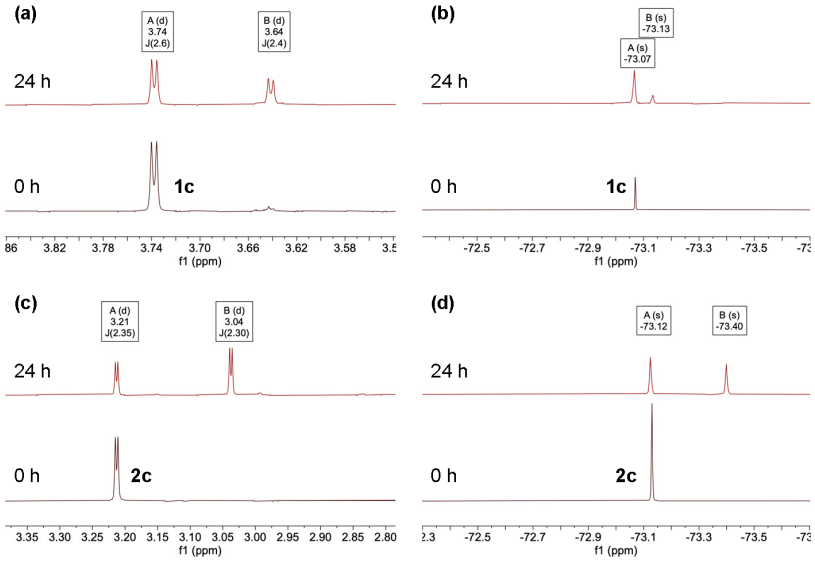

Figure 4. ^{1}H NMR and ^{19}F NMR spectra indicating the formation of [(FP)Rh(Me)(TFA)(CD_3CN)][TFA] (**1ci** and **2ci**) after 24 h. (a) ^{1}H NMR spectrum of **1c** in CD_3CN. (b) ^{19}F NMR spectrum of **1c** in CD_3CN. (c) ^{1}H NMR spectrum of **2c** in CD_3CN. (d) ^{19}F NMR spectrum of **2c** in CD_3CN.

Scheme 7. Proposed Equilibria between (FP)Rh(Me)(TFA)$_2$ (1c and 2c), CD_3CN and [(FP)Rh(Me)(TFA)(CD_3CN)][TFA] (1ci and 2ci)

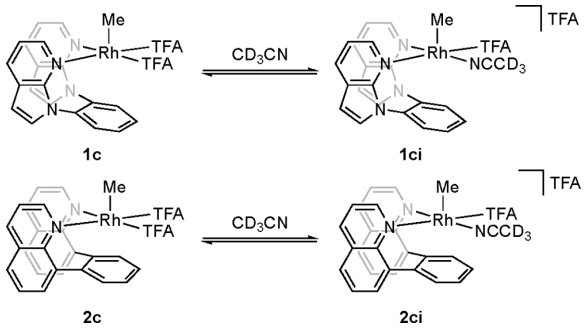

Table 3. Performance of Different (L)Rh(Me)(TFA)$_2$ Complexes (1c, 2c, 3c, 4c, and 5c) in Reductive Elimination of MeTFA in CD_3CN[a]

entry	complex	concentration (M)	temperature (°C)	reaction time (h)[b]	MeTFA yield
1	**1c**	0.01	90	48	59(1)%
2	**1c**[c]	0.005	90	48	49(1)%
3	**2c**	0.01	90	144	5(0)%
4	**3c**[c]	0.005	90	48	49(1)%
5	**4c**	0.01	90	48	2(0)%
6	**5c-NCMe**	0.01	90	48	12(1)%

[a]Reaction conditions: 0.5 mL CD_3CN, starting complex, 30 psig N_2. All yields are based on the average of at least three trials with standard deviations provided. [b]Reaction time refers to the time when highest yield is achieved. [c]Concentration of starting complex is 0.005 M.

facile, with a barrier of 24.6 kcal/mol. For **2ci** with the 6-FP ligand, we calculate a reductive elimination barrier of 44.6 kcal/mol and an S_N2 barrier of 25.1 kcal/mol. For both **1ci** and **2ci**, the reductive elimination barriers are very high and not a likely pathway for MeTFA formation, while S_N2 exhibits lower barriers for **1ci** and **2ci**, making it the favored pathway for production of MeTFA. The 24.6 kcal/mol S_N2 barrier for **1ci** is only 0.5 kcal/mol lower than the 25.1 kcal/mol S_N2 barrier for **2ci**, consistent with experimental observations (Table 3) that 5-FP complex gives a higher MeTFA yield than with 6-FP.

Figure 5 provides the DFT-optimized S_N2 transition states for **1ci** and **2ci**. The distances between the Rh center and the nearest carbons of the capping arene (C_c and C_B) in **1ci** transition state are 2.98 and 2.96 Å; the analogous distances for **2ci** are 2.90 and 2.76 Å. As observed previously, the 6-FP ligand provides closer Rh−arene interaction than the 5-FP ligand as indicated by the Rh−C_C and Rh−C_B distances. This difference in atom distances has a profound effect on the overall geometries of the S_N2 transition states as well as the relative free energies. In **1ci**, the Rh−C_{Me} bond has elongated to 2.25 Å, while the C_{Me}−O_{TFA} distance has shortened to 2.04 Å (where C_{Me} is the C of Me and O_{TFA} is the active O of TFA). In **2ci**, the Rh−C_{Me} is further elongated to 2.38 Å, while the C_{Me}−O_{TFA} distance is 1.97 Å. It is not immediately obvious from these distances that the **1ci** transition state provides a lower free energy barrier. The key descriptor for the S_N2 free energy barrier is the orientation of the Me relative to Rh and the external TFA, which can be described by the Rh−C_{Me}−O_{TFA} angle. In **1ci** transition state, the Rh−C_{Me}−O_{TFA} angle is 176°. In **2ci** transition state, the Rh−C_{Me}−O_{TFA} angle is 163°. The optimal angle for a S_N2 transition state is nominally 180°. Deviation from this angle results in an energy penalty due to imperfect orbital overlap. The Rh−C_{Me}−O_{TFA} angle in **1ci** only deviates from 180° by 4°, while **2ci** deviates by 17°. This significant deviation from the optimal S_N2 angle results in a less stable transition state and consequently a higher free energy barrier for **2ci**.

Effect of Additives on Reductive Elimination. Previously, we reported that the addition of ammonium

https://doi.org/10.1021/acs.organomet.1c00223
Organometallics 2021, 40, 1889−1906

Scheme 8. Calculated Free Energy Profiles (at 423 K) for MeTFA Formation via Reductive Elimination and Organometallic S_N2 Pathways from Rh^{III}–Me Complexes[a]

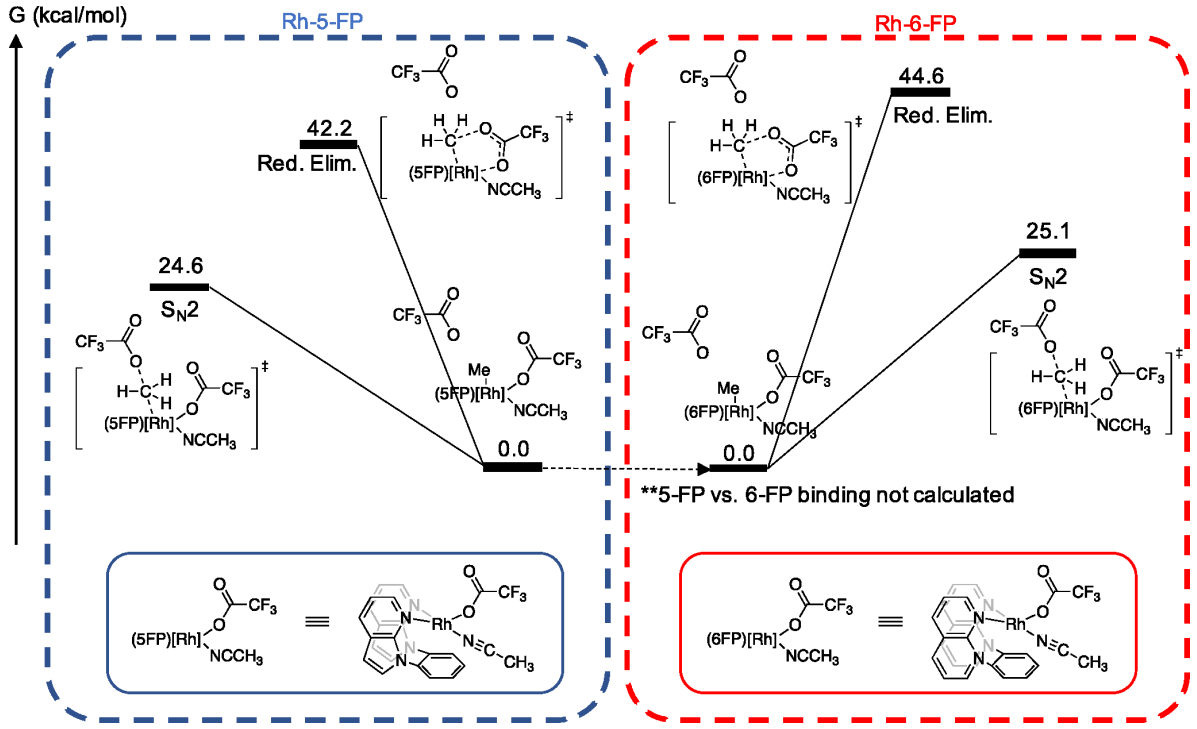

[a]We did not calculate the binding energies of the 5-FP and 6-FP ligands to Rh.

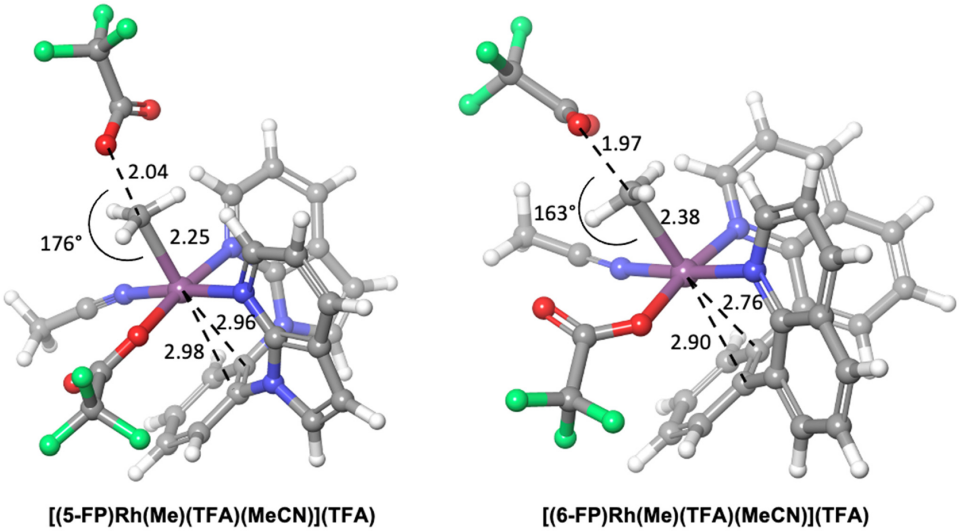

Figure 5. DFT-optimized structures of the transition states for Rh^{III}-Me reductive functionalization by bimolecular S_N2 pathways with the 5-FP (left) and 6-FP (right) ligands. All distances are in Å.

halide salts to solutions of Rh^{III} methyl complexes enhances reductive functionalization to form MeX,[27,28,53,54] but for **1c**, the addition of ammonium halide salts did not increase the yield of MeX (Table 4, entries 1–3). The addition of $[Bu_4N][Br]$ and $[Bu_4N][I]$ led to the formation of some MeBr and MeI, respectively (Table 4, entries 1 and 2). However, the addition of $[Bu_4N][Cl]$ did not lead to the formation of MeCl. These results indicate that the proposed S_N2 pathway is feasible through nucleophilic attack by I^- and Br^-, while the addition of Cl^- does not facilitate this reaction. In the case of **2c**, with added $[Bu_4N][I]$, the yield of MeTFA increased from 5(0)% to 20(1)% (Table 4, entry 4).

https://doi.org/10.1021/acs.organomet.1c00223
Organometallics 2021, 40, 1889–1906

Table 4. Effect of [Bu_4N][X] Additives (X = Halide) on Reductive Elimination of MeX from Rh Complexes[a]

entry	complex	additive	amount (equiv)	reaction time (h)[b]	yield of MeX[d]		
					MeTFA	MeX	total
1	**1c**	[Bu_4N][I]	2	84	33(2)%	14(2)% MeI	47(4)%
2	**1c**	[Bu_4N][Br]	2	84	5(0)%	24(5)% MeBr	29(5)%
3	**1c**	[Bu_4N][Cl]	2	84	N.D.	N.D.	N.D.
4	**2c**	[Bu_4N][I]	2	24	20(1)%	N.D.	20(1)%
5	**3c**[c]	[Bu_4N][I]	2	24	52(6)%	N.D.	52(6)%
6	**4c**	[Bu_4N][I]	2	24	15(2)%	N.D.	15(2)%

[a]Reaction conditions: 0.5 mL CD_3CN, 0.01 M starting complex (unless otherwise noted), 30 psig N_2, 90 °C. All yields are based on the average of at least three trials with standard deviations provided. [b]Reaction time refers to the time when highest yield is achieved under this condition for reactions generating MeX. [c]Using 0.005 M starting complex. [d]N.D. = not detected.

Table 5. Effect of Acid Additives ((Acetic Acid)-d_4 and D_2O) in the Reductive Functionalization of (5-FP)Rh(Me)$(TFA)_2$ (1c)[a]

entry	complex	temperature (°C)	reaction time (h)[b]	acid loading (μL)	yield of MeX[e]			
					MeOAc[c]	MeOD	MeTFA	total
1	**1c**	80	84	10 (DOAc)	11(1)%	N.D.	51(1)%	62(2)%
2	**1c**	80	84	20 (DOAc)	23(1)%	N.D.	36(3)%	59(3)%
3	**1c**	80	84	50 (DOAc)	42(3)%	N.D.	16(1)%	58(4)%
4[d]	**1c**	90	96	10 (D_2O)	N.D.	21(1)%	47(1)%	68(2)%
5	**1c**	90	24	100 (DOAc)	29(1)%	N.D.	29(5)%	58(6)%

[a]Reaction conditions: 0.5 mL CD_3CN, 0.01 M (5-FP)Rh(Me)$(TFA)_2$ (**1c**), (acetic acid)-d_4 (except entry 4), 30 psig N_2. All yields are based on the average of at least three trials with standard deviations provided. [b]Reaction times refer to the time when highest total yield of MeX is achieved under these conditions. [c]MeOAc refers to MeOAc-d_3, where the acetate is deuterated. [d]Reaction conditions: 0.5 mL CD_3CN, 0.01 M **1c**, D_2O, 30 psig N_2. [e]N.D. = not detected.

Reductive Elimination under Acidic Conditions. (Acetic acid)-d_4 and D_2O were used to investigate the effect of protic additives on reductive elimination from **1c**. In all cases, the addition of acid had no obvious effect on overall yields (Table 5). The major effect of (acetic acid)-d_4 is that it shifts the MeX formation from MeTFA to MeOAc-d_3. The ratio of MeTFA to MeOAc-d_3 decreases from 5:1 to 1:1 when the acetic acid addition increases from 10 to 50 μL. The addition of a large amount of acid appears to slightly accelerate the reaction (Entry 5). Also, the addition of water increases the total MeX yield to a similar extent as acetic acid, and the formation of MeOD was observed (entry 4).

Oxidatively Induced Reductive Functionalization. We tested the impact of Ag^I and Ag^{II} salts and found that AgF, AgF_2, AgOTf, and AgTFA facilitate reductive elimination (Tables 6 and S4).[57,58,71−74] In the case of AgOTf, the yield of MeTFA was 87(1)% after 96 h of reaction (Table 6, entry 4). A control experiment using KOTf gives no improvement in the yield of MeTFA (entry 9) and no observation of MeOTf formation, suggesting that the major contribution to reductive elimination was the oxidative effect of Ag^I oxidant rather than increased concentration of OTf^-. Also, $K_2S_2O_8$ was shown to facilitate reductive functionalization, achieving a yield of 76(1)% after 72 h (entry 8). We speculated that the poor solubility of $K_2S_2O_8$ in CD_3CN might prevent a higher yield; however, the addition of [Et_4N][BF_4], a phase transfer catalyst, did not lead to an improvement in reaction rate or MeTFA yield (entry 9). The addition of 2 equiv of AgOTf also facilitates MeX reductive eliminations from **2c**, **3c**, **4c**, and **5c** (entries 11, 12, 14, and 15).

To aid in determining whether the oxidatively induced reductive elimination operates through a $2e^-$ oxidation mechanism followed by Rh^V/Rh^{III} reductive elimination or a $1e^-$ oxidation followed by Rh^{IV}/Rh^{II} reductive elimination

Table 6. Facilitation of Reductive Elimination Using Oxidant Additives[a]

entry	complex	additive	amount (equiv)	reaction time (h)[b]	yield of MeTFA
1	**1c**	AgF	2	48	68(2)%
2	**1c**	AgF_2	2	48	72(1)%
3	**1c**	AgOTf	1	96	87(5)%
4	**1c**	AgOTf	2	96	87(1)%
5[c]	**1c**	AgOTf	2	96	78(2)%
6	**1c**	AgOTf	4	96	85(1)%
7	**1c**	AgTFA	2	48	72(1)%
8	**1c**	$K_2S_2O_8$	2	48	76(1)%
9	**1c**	$K_2S_2O_8$ + NEt_4BF_4	2 + 2	48	72(3)%
10	**1c**	KOTf	2	48	42(3)%
11	**2c**	AgOTf	2	144	8(0)%
12[c]	**3c**	AgOTf	2	96	62(6)%
13[c]	**3c**	$K_2S_2O_8$	2	48	56(2)%
14	**4c**	AgOTf	2	144	15(1)%
15	**5c-NCMe**	AgOTf	2	48	21(3)%

[a]Reaction conditions: 0.5 mL CD_3CN, 0.01 M starting complex (unless otherwise noted), additive, 30 psig N_2, 90 °C. All yields are based on the average of at least three trials with standard deviations provided. [b]Reaction times refer to the time when highest yield of MeTFA is achieved under these conditions. [c]Using 0.005 M starting complex.

(Scheme 9), we added varied amounts of AgOTf to observe the impact on MeX yield (Table 6, entries 3, 4, and 6). Theoretically, when using only 1 equiv of AgOTf, the maximum yield of MeTFA is 50% for a $2e^-$ oxidation but 100% for a $1e^-$ oxidation.[74] The addition of 1 equiv of AgOTf produces a MeTFA yield of 87(5)% (entry 3), which is

https://doi.org/10.1021/acs.organomet.1c00223
Organometallics 2021, 40, 1889−1906

Scheme 9. Possible Mechanisms of Two-Electron Oxidation Followed by Rh^{V}/Rh^{III} Reductive Elimination (Blue) and One-Electron Oxidation Followed by Rh^{IV}/Rh^{II} Reductive Elimination (Red)

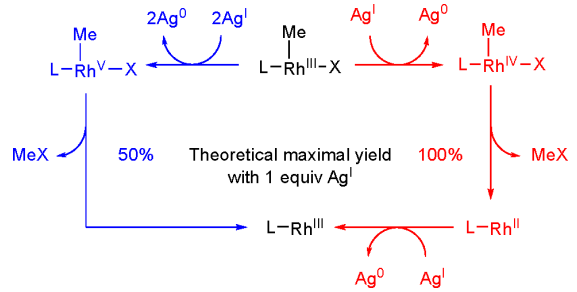

consistent with a reaction pathway involving a $1e^-$ oxidation to form Rh^{IV}. Further increasing the amount of oxidant did not result in an increase in the yield (entry 6), consistent with this conclusion.

Cyclic voltammetry experiments for (5-FP)Rh(Me)$(TFA)_2$ (**1c**) were conducted (Figure 6). The cyclic voltammogram of

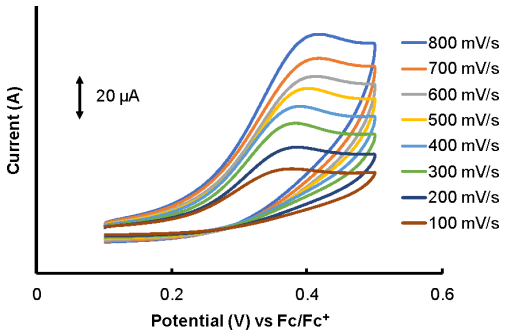

Figure 6. Narrow potential window CVs of $Rh^{III/IV}$ at various scan rates.

1c displayed a single irreversible oxidation peak at E_{pa} = 0.38 V (vs Fc^+/Fc, 100 mV/s) (Figure S53). Observed peaks at 0.94 and 1.10 V are possibly due to ligand oxidation (see the Supporting Information). The potential of Ag^+/Ag is 0.41 V (vs Fc^+/Fc), and the potential of $S_2O_8^{2-}/SO_4^{2-}$ is 1.61 V. This may explain why Ag^I salts and $K_2S_2O_8$ are able to facilitate the MeTFA reductive elimination from **1c**, but Cu^{II} salts (Cu^{2+}/Cu^+: −0.25 V) and Fe^{III} salts (Fe^{3+}/Fe^{2+}: 0.37 V) cannot.

To confirm our prediction of oxidatively induced reductive elimination via a $1e^-$ oxidation pathway, we applied DFT calculations to the mechanisms in Scheme 8. Beginning with **1ci** and **2ci**, we first investigated $1e^-$ and $2e^-$ oxidations of Rh^{III} to Rh^{IV} and Rh^{V} using equivalents of AgOTf (Scheme 10a and 10b). One consideration is that the reduction of AgOTf to atomic Ag^0 will be uphill, but the cohesive energy of Ag^0 congregating to form Ag precipitate (observed experimentally) is downhill 67.9 kcal/mol. Due to the challenges in accurately calculating $Rh^{III} + Ag^I \rightarrow Rh^{IV} + Ag$, we focused only on the Rh^{V} and Rh^{IV} starting states and set the Rh^{IV} complexes at 0.0 kcal/mol in Scheme 10. More details on the relative energies of $Rh^{III}/Rh^{IV}/Rh^{V}$ can be found in the Supporting Information.

Relative to the Rh^{IV} intermediate: (a) DFT predicts a 14.2 kcal/mol S_N2 barrier for MeTFA reductive elimination from $[(5\text{-FP})Rh^{IV}(Me)(TFA)_2][OTf]$ to form $(5\text{-FP})Rh^{II}(TFA)(OTf)$. (b) For S_N2 reduction elimination from $[(6\text{-FP})Rh^{IV}(Me)(TFA)_2][OTf]$ to form MeTFA and $(6\text{-FP})Rh^{II}(TFA)(OTf)$, DFT predicts a barrier of 15.9 kcal/mol.

Relative to their Rh^{IV} starting states: (a) $(5\text{-FP})Rh^{II}(TFA)(OTf)$ is 52.9 kcal/mol downhill. (b) $(6\text{-FP})Rh^{II}(TFA)(OTf)$ is 74.7 kcal/mol downhill, indicating that the Rh^{IV}/Rh^{II} reductive elimination is highly exergonic. (c) For the 5-FP ligand, the Rh^{IV} S_N2 barrier is 10.4 kcal/mol lower than the 24.6 kcal/mol Rh^{III} S_N2 barrier. (d) With the 6-FP ligand, the Rh^{IV} S_N2 barrier is 9.2 kcal/mol lower than the 25.1 kcal/mol Rh^{III} barrier. Similar to the Rh^{III} cases, the Rh^{IV} S_N2 barrier with the 5-FP ligand is 1.7 kcal/mol lower than the barrier with the 6-FP ligand.

For the $2e^-$ oxidation pathway, we began by attempting to locate the intermediate states for $(5\text{-FP})Rh^{V}(Me)(TFA)_2(OTf)_2$ and $(6\text{-FP})Rh^{V}(Me)(TFA)_2(OTf)_2$. However, computationally we found these Rh^{V} states to be computationally unstable. The acetonitrile ligand binds strongly to the Rh^{V} center, so one TFA ligand and both OTf ligands must remain farther from Rh in the solvent shell. This abundance of charged ligands in the solvent shell leads to unwanted nucleophilic attack by the charged OTf ligands on the FP ligand. Consequently, we were unable to locate stable Rh^{V} species or their subsequent S_N2 transition states. This result is not surprising; previous attempts to isolate the +5 oxidation state of group 9 metals (namely Rh and Ir) has proved difficult and only possible in the presence of strong oxidants.[75,76] These results are consistent with our proposal that the oxidatively induced reductive elimination reactions likely occur through the $1e^-$ oxidation involving Rh^{IV}. Additionally, our findings agree with a previous study by Chang and co-workers in which the Rh^{IV}/Rh^{II} reductive elimination yielded a lower barrier and more exergonic reaction than the Rh^{III}/Rh^{I} reductive elimination.[58]

CONCLUSIONS

We speculated that occupying one of the coordination sites of Rh^{III} centers with a weakly donating or nondonating group could prevent the formation of a saturated 18-electron structure, thus destabilizing the Rh^{III} oxidation state and facilitating reductive elimination. Our strategy to test this hypothesis involved the use of capping arene ligands [8,8′-(1,2-arene)diquinoline and 1,2-bis(*N*-7-azaindolyl)arene], where the Rh−arene interaction can be tuned by the structure of the ligand. Four capping arene ligated Rh^{III}−Me complexes with different metal−arene distances were synthesized. The 5-FP Rh^{III} complexes, with reduced Rh−arene interaction (as evidenced by longer $Rh-C_{arene}$ bond distances from solid-state X-ray structures) compared to the analogous 6-FP Rh^{III} complexes demonstrate enhanced yields of MeX formation. In contrast, the two 6-FP Rh^{III} methyl complexes only form MeTFA in low (<10%) yield. Furthermore, a related example with the dpe ligand, $(dpe)Rh(Me)(TFA)_2$ (**5c**), gives the performance in reductive elimination better than 6-^{X}FP complexes but worse than 5-^{X}FP complexes. Computational and experimental studies are consistent with an S_N2 pathway for MeTFA formation from [(5-FP)Rh(Me)(TFA)(NCMe)][TFA] complexes.

Another strategy applied in this work is the use of oxidants to induce reductive functionalization. Select Ag^I or Ag^{II}

https://doi.org/10.1021/acs.organomet.1c00223
Organometallics 2021, 40, 1889−1906

Scheme 10. Calculated Free Energy Profiles for MeTFA Formation via Reductive Elimination from Rh^{IV} Intermediates

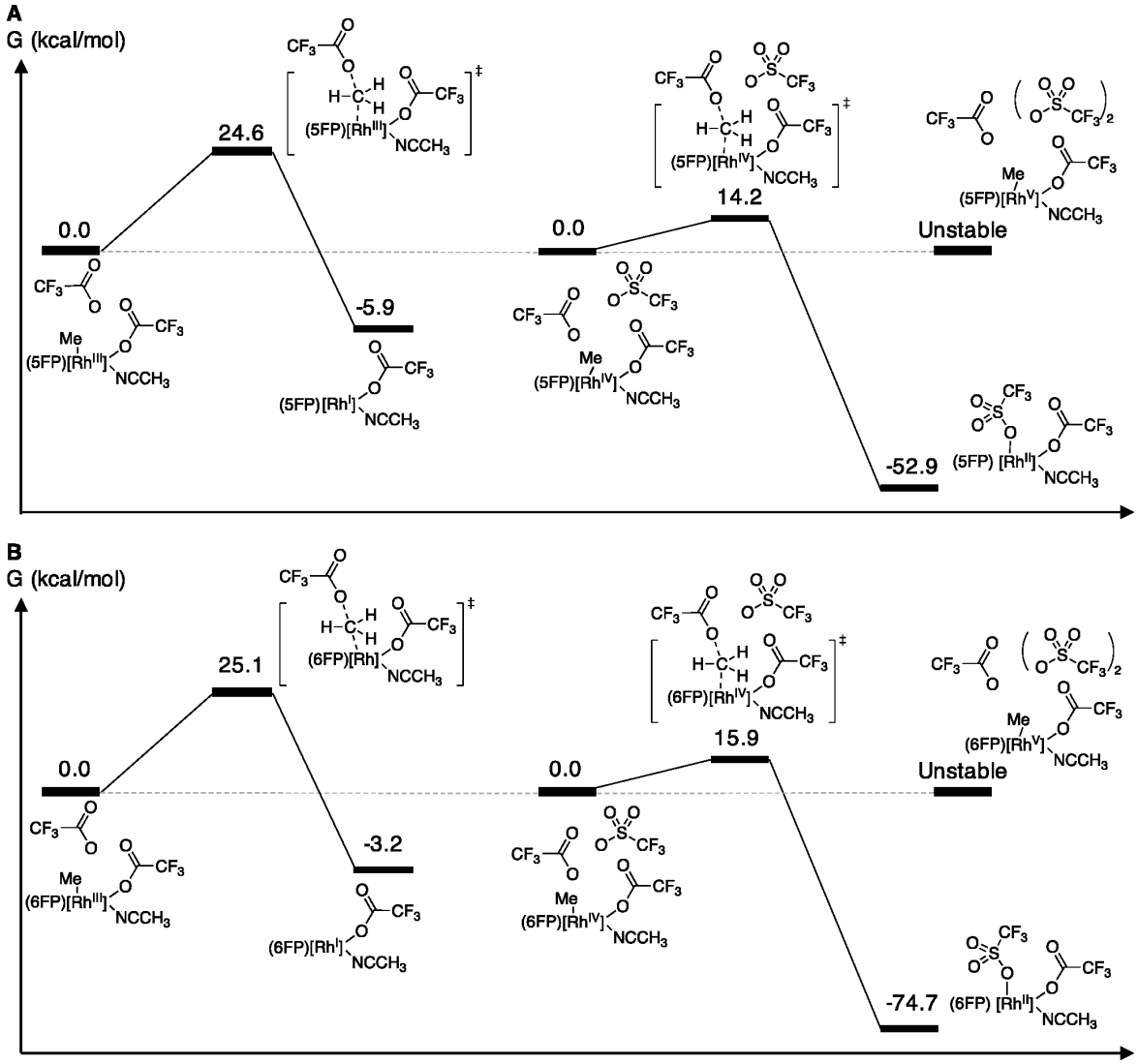

oxidants and $K_2S_2O_8$ were discovered to promote the formation of MeX. With AgOTf as the oxidant, the MeTFA yield is 87(2)%. A mechanism of $1e^-$ oxidation of Rh^{III}–Me complex followed by Rh^{IV}/Rh^{II} reductive elimination is proposed and supported by cyclic voltammetry and DFT calculations.

This research presents a new ligand-based strategy for the promotion of reductive functionalization of MeX from Rh^{III}–Me complexes, a key step in possible Rh-catalyzed functionalization of light alkanes (Scheme 1). With the application of the capping arene and the single-electron oxidant AgOTf, we have been able to achieve MeTFA yield as high as 87%.

EXPERIMENTAL SECTION

General Methods. Unless otherwise noted, all reactions and manipulations were performed under a dinitrogen atmosphere in a glovebox or using standard Schlenk techniques with dried and degassed solvents. All protio and deuterated solvents were stored in the glovebox over 4 Å molecular sieves. All NMR spectra were recorded on Varian Inova 600 or 500 MHz spectrometer or Bruker Avance III 800 MHz spectrometer. The operating frequency for $^{13}C\{^1H\}$ NMR spectroscopy is 150 MHz (on 600 MHz instrument) or 201 MHz (on 800 MHz instrument). For ^{19}F NMR spectroscopy ,the operating frequency is 564 MHz (on 600 MHz instrument). All ^1H and $^{13}C\{^1H\}$ NMR spectra are referenced against residual ^1H resonances (^1H NMR) or the $^{13}C\{^1H\}$ resonances ($^{13}C\{^1H\}$ NMR) of the deuterated solvents. ^{19}F NMR spectra were referenced against the resonance of C_6F_6. All spectra were recorded at 25 °C unless otherwise indicated. Literature procedures were used to prepare 5-FP (**1**), dpe (**5**), and $[Rh(\eta^2\text{-}C_2H_4)_2(\mu\text{-}Cl)]_2$.[63,64,77]

Synthesis and Characterization. *(5-FP)Rh(Cl)(η^2-C_2H_4) (**1a**).*

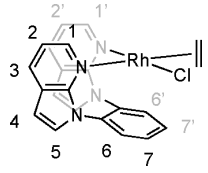

https://doi.org/10.1021/acs.organomet.1c00223
Organometallics 2021, 40, 1889−1906

A THF solution (10 mL) of 5-FP (**1**) (81.0 mg, 261 μmol) was added dropwise to a THF solution (10 mL) of $[Rh(\eta^2\text{-}C_2H_4)_2(\mu\text{-}Cl)]_2$ (57.2 mg, 147 μmol) and stirred at room temperature for 24 h. Then, the reaction mixture was concentrated under vacuum to yield a crude product. The resulting solid was dissolved in minimal amount of THF (4 mL), and pentane (30 mL) was added to the solution to give a brown precipitate. The solid was collected by filtration, washed with pentane (3 × 10 mL), and dried under vacuum to afford (5-FP)Rh(Cl)(η^2-C_2H_4) (89.0 mg, yield = 70%). X-ray quality crystals of (5-FP)Rh(Cl)(η^2-C_2H_4) (**1a**) were obtained by slow vapor diffusion of *n*-pentane into a solution of complex **1a** in THF. ^{1}H NMR (600 MHz, CD_2Cl_2): δ 8.96 (dd, $^3J_{HH}$ = 5 Hz, $^4J_{HH}$ = 1 Hz, 1H, 1 or 1′), 8.46 (d, $^3J_{HH}$ = 5 Hz, $^4J_{HH}$ = 1H, 1 or 1′), 7.89−7.80 (m, 3H, three of 6, 6′, 7, 7′), 7.78 (dd, $^3J_{HH}$ = 8 Hz, $^4J_{HH}$ = 1H, 3 or 3′), 7.60 (dd, $^3J_{HH}$ = 8 Hz, $^4J_{HH}$ = 1 Hz, 1H, 3 or 3′), 7.50−7.42 (m, 1H, one of 6, 6′, 7, 7′), 7.27 (d, $^3J_{HH}$ = 4 Hz, 1H, 4, 4′, 5, or 5′), 7.23 (d, $^3J_{HH}$ = 4 Hz, 1H, 4, 4′, 5, or 5′), 7.06 (dd, $^3J_{HH}$ = 8, 5 Hz, 1H, 2 or 2′), 6.75 (dd, $^3J_{HH}$ = 8, 5 Hz, 1H, 2 or 2′), 6.47 (d, $^3J_{HH}$ = 4 Hz, 1H, 4, 4′, 5, or 5′), 6.45 (d, $^3J_{HH}$ = 4 Hz, 1H, 4, 4′, 5, or 5′), 2.72 (br, 2H, C_2H_4), 2.47 (br, 2H, C_2H_4). $^{13}C\{^1H\}$ NMR (201 MHz, CD_2Cl_2): δ 151.8 (s), 150.0 (s), 148.6 (s), 144.9 (s), 136.3 (s), 135.6 (s), 132.3 (s), 131.4 (s), 131.0 (s), 131.0 (s), 130.6 (s), 130.4 (s), 130.0 (s), 128.9 (s), 122.2 (s), 121.5 (s), 117.5 (s), 117.0 (s), 103.0 (s), 102.8 (s), 50.3 (br, C_2H_4). Acceptable elemental analysis results for **1a** could not be obtained. The NMR spectra of **1a** appear in Figures S1 and S2.

*(5-FP)Rh(Me)(X)(X′) (X = Cl or I) (**1b**).* Iodomethane (0.5 mL) was added dropwise to a THF solution (30 mL) of (5-FP)Rh(Cl)(η^2-C_2H_4) (**1a**) (111 mg, 232 μmol) and stirred at room temperature for 48 h. The reaction mixture was concentrated under vacuum to yield crude solid product. The resulting solid was dissolved in minimal THF (4 mL), and pentane (30 mL) was added to the solution to give a yellow precipitate. The solid was collected by filtration, washed with pentane (3 × 10 mL), and dried under vacuum to afford a mixture of (5-FP)Rh(Me)(X)(X′) (101 mg). The ^{1}H NMR spectrum is provided in Figure S3.

*(5-FP)Rh(Me)(TFA)$_2$ (**1c**).*

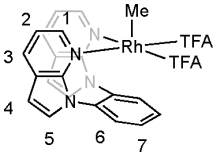

A THF solution (30 mL) of (5-FP)Rh(Me)(X)(X′) (**1b**) (121 mg) was prepared, and AgTFA (90.6 mg, 410 μmol) was added to the solution, which was shielded from light using aluminum foil. After stirring for 24 h, the reaction mixture was filtered through Celite. The filtrate was concentrated under vacuum. The resulting solid was dissolved in minimal THF (4 mL), and pentane (30 mL) was added to the solution to give a white precipitate. The solid was collected by filtration, washed with pentane (3 × 10 mL), and dried under vacuum to afford (5-FP)Rh(Me)$(TFA)_2$ (127 mg, yield = 95%). X-ray quality crystals of (5-FP)Rh(Me)$(TFA)_2$ (**1c**) were obtained by slow vapor diffusion of *n*-pentane into a solution of complex **1c** in THF. ^{1}H NMR (497 MHz, CD_2Cl_2): δ 8.32 (d, $^3J_{HH}$ = 6 Hz, 2H, 1), 7.92−7.86 (m, 4H, 3 and 6 or 7), 7.69 (dd, $^3J_{HH}$ = 7, 5 Hz, 2H, 6 or 7), 7.25 (d, $^3J_{HH}$ = 4 Hz, 2H, 4 or 5), 7.08 (dd, $^3J_{HH}$ = 8, 6 Hz, 2H, 2), 6.64 (d, $^3J_{HH}$ = 4 Hz, 2H, 4 or 5), 3.82 (d, $^2J_{RhH}$ = 3 Hz, 3H, CH_3). $^{13}C\{^1H\}$ NMR (150 MHz, CD_2Cl_2): δ 162.3 (q, $^2J_{FC}$ = 36 Hz, $COCF_3$), 153.4, 145.5, 133.7, 133.6, 132.9, 131.8, 130.4, 122.5, 117.5, 113.3 (q, $^1J_{FC}$ = 292 Hz, $COCF_3$), 104.6, 23.6 (d, $^1J_{RhC}$ = 27 Hz, CH_3). ^{19}F NMR (564 MHz, CD_2Cl_2): δ −73.8. Anal. Calcd for $C_{25}H_{17}F_6N_4O_4Rh$: C, 45.89; H, 2.62; N, 8.56. Found: C, 46.11; H, 2.60; N, 8.66.

*6-FP (8,8′-(1,2-phenylene)diquinoline) (**2**).*

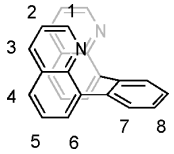

The procedure was modified from reported procedures of similar compounds.[59,62] Quinolin-8-ylboronic acid (3.00 g, 17.3 mmol, 2.4 equiv), 1,2-diiodobenzene (2.39 g, 7.24 mmol, 1 equiv), K_3PO_4 (34.0 g, 159 mmol, 22 equiv), and $Pd(PPh_3)_4$ (0.81 g, 0.72 mmol, 0.1 equiv) were combined in a 500 mL Schlenk flask. Under an inert atmosphere, degassed DMF (60 mL) and degassed DI water (60 mL) were added to the Schlenk flask, and the flask was fitted with a glass stopper and sealed. The glass stopper was secured to the Schlenk flask with several rubber bands, and then the reaction mixture was heated in an oil bath at 115 °C with stirring for 24 h. The reaction mixture was allowed to cool to room temperature, during which the aqueous and organic layers separated. The lower aqueous phase was separated from the organic phase and discarded. The organic layer was collected, and a copious amount of DI water (500 mL) was added to precipitate a yellow oily solid. The solid was collected by filtration, dissolved in Et_2O (30 mL), and filtered. The filtrate was collected and reduced under mild pressure to an oil. The product was purified by column chromatography using silica gel as the immobilized phase. A mixture of hexanes and ethyl acetate (5:1 *v*/*v*, then 3:1) with a few drops of triethylamine was used as the eluent. The product fraction was collected and activated charcoal was added, turning the yellow solution to colorless. The solvent was removed under vacuum, affording a colorless oil. The product was dried under vacuum, washed with pentane, and then filtered to obtain 6-FP (**2**) as a white powder. The isolated yield is 85% (2.05 g). X-ray quality crystals of 6-FP (**2**) were obtained by slow vapor diffusion of *n*-pentane into a solution of **2** in THF. ^{1}H NMR (800 MHz, C_6D_6): δ 8.72 (br, 2H, 1), 7.77 (dd, AA′BB′, $^3J_{HH}$ = 7, 5 Hz, 2H, 7 or 8), 7.53 (d, $^3J_{HH}$ = 7 Hz, 2H, 4 or 6), 7.41 (br, 2H, 3), 7.38 (dd, AA′BB′, $^3J_{HH}$ = 7, 5 Hz, 7 or 8), 7.08 (dd, $^3J_{HH}$ = 8 Hz, $^4J_{HH}$ = 1 Hz, 2H, 4 or 6), 6.75 (br, 2H, 5), 6.71 (br, 2H, 2). $^{13}C\{^1H\}$ NMR (201 MHz, C_6D_6): δ 149.8 (br), 147.6 (br), 142.4 (s), 140.3 (s), 135.5 (br), 132.4 (s), 131.3 (s), 128.4 (s), 126.9 (s), 126.7 (s), 125.7 (s), 120.7 (s). Anal. Calcd for $C_{24}H_{16}N_2$: C, 86.72; H, 4.85; N, 8.43. Found: C, 86.44; H, 4.84; N, 8.41.

*(6-FP)Rh(Cl)(η^2-C_2H_4) (**2a**).*

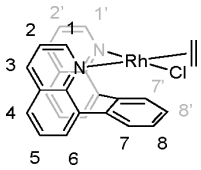

A THF solution (30 mL) of 6-FP (**2**) (228 mg, 686 μmol) was added dropwise to a THF solution (70 mL) of $[Rh(\eta^2\text{-}C_2H_4)_2(\mu\text{-}Cl)]_2$ (134 mg, 343 μmol) and stirred for 24 h. The reaction mixture was dried under vacuum. The resulting solid was dissolved in minimal amount of DCM, and pentane (50 mL) was added to the solution to give a red precipitate. The solid was collected by filtration, washed with pentane (3 × 20 mL), and dried under vacuum to afford the analytically pure product (6-FP)Rh(Cl)(η^2-C_2H_4) (304 mg, isolated yield = 89%). X-ray quality crystals of (6-FP)Rh(Cl)(η^2-C_2H_4) (**2a**) were obtained by slow vapor diffusion of *n*-pentane into a solution of complex **2a** in THF. ^{1}H NMR (600 MHz, CD_2Cl_2): δ 9.91 (dd, $^3J_{HH}$ = 5 Hz, $^4J_{HH}$ = 2 Hz, 1H, 1 or 1′), 8.58 (d, $^3J_{HH}$ = 5 Hz, 1H, 1 or 1′), 8.09 (dd, $^3J_{HH}$ = 8 Hz, $^4J_{HH}$ = 2 Hz, 1H, 3 or 3′), 8.01 (d, $^3J_{HH}$ = 8 Hz, 1H, 3 or 3′), 7.78 (dd, $^3J_{HH}$ = 7 Hz, $^4J_{HH}$ = 2 Hz, 1H, 4 or 4′), 7.75 (dd, $^3J_{HH}$ = 8 Hz, $^4J_{HH}$ = 2 Hz, 1H, 4 or 4′), 7.64−7.58 (m, 1H, one of 7, 7′, 8 and 8′), 7.57−7.46 (m, 5H, three of 7, 7′, 8, and 8′; 5 and 5′), 7.21−7.14 (m, 2H, 2 or 2′ and 6 or 6′), 7.11 (d, $^3J_{HH}$ = 8 Hz, 1H, 6 or 6′), 6.78 (dd, $^3J_{HH}$ = 8, 5 Hz, 1H, 2 or 2′), 3.55 (br, 1H, C_2H_4), 2.32 (br, 1H, C_2H_4), 1.80

https://doi.org/10.1021/acs.organomet.1c00223
Organometallics 2021, 40, 1889−1906

(br, 1H, C_2H_4), 1.53 (br, 1H, C_2H_4). $^{13}C\{^1H\}$ NMR (201 MHz, CD_2Cl_2): δ 155.3, 154.3, 151.2, 149.2, 141.6, 140.5, 136.9, 135.6, 134.2, 133.8, 132.0, 131.9, 129.8, 129.8, 129.2, 128.9, 128.1, 127.6 (2C), 127.3, 127.2, 126.6, 121.6, 121.5, 45.9 (br, C_2H_4), 35.4 (br, C_2H_4). Anal. Calcd for $C_{26}H_{20}ClN_2Rh$: C, 62.60; H, 4.04; N, 5.62. Found: C, 62.97; H, 4.23; N, 5.54.

(6-FP)Rh(Me)(X)(X′) (**2b**). Iodomethane (1 mL) was added dropwise to a THF solution (100 mL) of (6-FP)Rh(Cl)(η^2-C_2H_4) (**2a**) (304 mg, 610 μmol) and stirred for 24 h. The reaction mixture was concentrated under vacuum. The resulting solid was dissolved in a minimal amount of DCM, and pentane (100 mL) was added to the solution to give a yellow precipitate. The solid was collected by filtration, washed with pentane (3 × 20 mL), and dried under vacuum to afford a mixture of (6-FP)Rh(Me)(X)(X′) (270 mg). The ^1H NMR spectrum is provided in Figure S14.

(6-FP)Rh(Me)(TFA)$_2$ (**2c**).

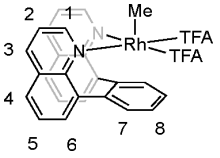

A THF solution (100 mL) of (6-FP)Rh(Me)(X)(X′) (**2b**) (271 mg) was prepared, and AgTFA (199 mg, 901 μmol) was added to the solution, which was shielded from light using aluminum foil. After stirring for 24 h, the reaction mixture was filtered through Celite. The filtrate was dried under vacuum. The resulting solid was dissolved in a minimal amount of DCM (5 mL), and pentane (150 mL) was added to the solution to give a white precipitate. The solid was collected by filtration, washed with pentane (3 × 10 mL), and dried under vacuum to afford analytically pure (6-FP)Rh(Me)-$(TFA)_2$ (290 mg, yield = 97%). X-ray quality crystals of (6-FP)Rh(Me)$(TFA)_2$ (**2c**) were obtained by slow vapor diffusion of *n*-pentane into a solution of complex **2c** in THF. ^1H NMR (600 MHz, CD_2Cl_2): δ 8.82 (d, $^3J_{HH}$ = 5 Hz, 2H, 1), 8.14 (dd, $^3J_{HH}$ = 8 Hz, $^4J_{HH}$ = 2 Hz, 2H, 3), 7.78 (dd, AA′BB′, $^3J_{HH}$ = 7, 6 Hz, 2H, 7 or 8), 7.65 (m, 4H, 4 or 6 and 7 or 8), 7.51−7.43 (m, 4H, 5 and 4 or 6), 7.31 (dd, $^3J_{HH}$ = 8, 5 Hz, 2H, 2), 3.28 (d, $^2J_{RhH}$ = 2 Hz, 3H, CH_3). $^{13}C\{^1H\}$ NMR (150 MHz, CD_2Cl_2): δ 162.6 (q, $^2J_{FC}$ = 35 Hz, $COCF_3$), 156.4, 151.4, 139.6, 137.7, 135.3, 134.0, 133.7, 131.3, 129.2, 128.7, 127.6, 122.0, 114.0 (q, $^1J_{FC}$ = 291 Hz, $COCF_3$), 23.6 (d, $^1J_{RhC}$ = 27 Hz, CH_3). ^{19}F NMR (564 MHz, CD_2Cl_2): δ −73.9 (s, TFA). Anal. Calcd for $C_{29}H_{19}F_6N_2O_4Rh$: C, 51.50; H, 2.83; N, 4.14. Found: C, 50.60; H, 2.67; N, 4.05.

5-^{NP}FP (2,3-bis(N-7-azaindolyl)naphthalene) (**3**).

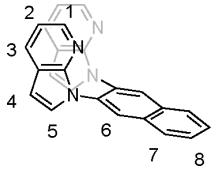

In a 100 mL pressure flask, 7-azaindole (1.30 g, 11 mmol), 2,3-dibromonaphthlene (1.31 g, 4.58 mmol), CuI (0.17 g, 0.9 mmol), 1,10-phenanthroline (0.32 g, 1.8 mmol), Cs_2CO_3 (6.2 g, 19 mmol), and dodecane (0.45 mL) were mixed in 10 mL of DMF. The pressure flask was sealed, taken out of the glovebox, and heated at 150 °C for 6 days. After allowing the flask to cool to room temperature, the mixture was diluted with 20 mL of DCM and filtered through a plug of silica gel. The filtrate was concentrated under vacuum, and the residue was flushed through a silica gel column with hexanes and ethyl acetate (3:1 *v*/*v*) as the eluent. The solvent was removed, resulting in a yellow oil. The oil was dissolved in minimal amount of DCM and flushed through a silica gel column using hexanes and ethyl acetate (10:1, 5:1, and then 3:1 *v*/*v*) as the eluent. Multiple fractions were collected, and 5-^{NP}FP was isolated upon solvent removal in vacuo. The isolated yield is 890 mg (yield = 54%). X-ray quality crystals of 5-^{NP}FP (**3**) were obtained by the bilayer diffusion using benzene and hexanes. ^1H NMR (600 MHz, CD_2Cl_2): δ 8.22 (s, 2H, 6), 8.14 (dd, $^3J_{HH}$ = 5 Hz, $^4J_{HH}$ = 2 Hz, 2H, 1), 8.01 (dd, AA′BB′, $^3J_{HH}$ = 7, 5 Hz, 2H, 7 or 8), 7.83 (dd, $^3J_{HH}$ = 8 Hz, $^4J_{HH}$ = 2 Hz, 2H, 3), 7.64 (dd, AA′BB′, $^3J_{HH}$ = 7, 5 Hz, 2H, 7 or 8), 7.03 (dd, $^3J_{HH}$ = 8, 5 Hz, 2H, 2), 6.93 (d, $^3J_{HH}$ = 4 Hz, 2H, 4 or 5), 6.30 (d, $^3J_{HH}$ = 4 Hz, 2H, 4 or 5). $^{13}C\{^1H\}$ NMR (201 MHz, CD_2Cl_2): δ 149.1, 143.9, 133.1, 133.1, 129.3, 129.0, 128.6, 128.4, 127.8, 120.9, 117.0, 101.6. Anal. Calcd for $C_{24}H_{16}N_4$: C, 79.98; H, 4.47; N, 15.55. Found: C, 80.08; H, 4.52; N, 15.48.

(5-^{NP}FP)Rh(Cl)(η^2-C_2H_4) (**3a**).

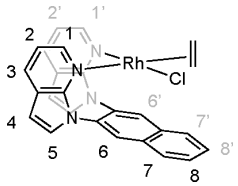

A THF solution (10 mL) of 2,3-bis(*N*-7-azaindolyl)naphthalene (5-^{NP}FP, 36.0 mg, 100 μmol) was added dropwise to a THF solution (20 mL) of $[Rh(\eta^2\text{-}C_2H_4)_2(\mu\text{-}Cl)]_2$ (19.0 mg, 50 μmol) and stirred for 24 h. The reaction mixture was dried under vacuum. The resulting solid was dissolved in minimal amount of DCM, and pentane (50 mL) was added to the solution to give a brown precipitate. The solid was collected by filtration, washed with pentane (3 × 10 mL), and dried under vacuum to afford (5-^{NP}FP)Rh(Cl)(η^2-C_2H_4) (42 mg, isolated yield = 79%). X-ray quality crystals of (5-^{NP}FP)Rh(Cl)(η^2-C_2H_4) (**3a**) were obtained by slow vapor diffusion of *n*-pentane into a solution of complex **3a** in THF. ^1H NMR (600 MHz, CD_2Cl_2): δ 8.91 (dd, $^3J_{HH}$ = 5 Hz, $^4J_{HH}$ = 1 Hz, 1H, 1 or 1′), 8.46 (d, $^3J_{HH}$ = 6 Hz, 1H, 1 or 1′), 8.26 (s, 1H, 6 or 6′), 8.10 (d, $^3J_{HH}$ = 8 Hz, 1H, 7, 7′, 8, or 8′), 8.04 (d, $^3J_{HH}$ = 8 Hz, 1H, 7, 7′, 8, or 8′), 7.99 (s, 1H, 6 or 6′), 7.80 (dd, $^3J_{HH}$ = 8 Hz, $^4J_{HH}$ = 1 Hz, 1H, 3 or 3′), 7.76−7.69 (m, 2H, two of 7, 7′, 8, or 8′), 7.62 (dd, $^3J_{HH}$ = 8 Hz, $^4J_{HH}$ = 1 Hz, 1H, 3 or 3′), 7.35 (d, $^3J_{HH}$ = 4 Hz, 1H, 4, 4′, 5, or 5′), 7.32 (d, $^3J_{HH}$ = 4 Hz, 1H, 4, 4′, 5, or 5′), 7.07 (dd, $^3J_{HH}$ = 8, 5 Hz, 1H, 2 or 2′), 6.77 (dd, $^3J_{HH}$ = 8, 5 Hz, 1H, 2 or 2′), 6.50 (d, $^3J_{HH}$ = 4 Hz, 1H, 4, 4′, 5, or 5′), 6.46 (d, $^3J_{HH}$ = 4 Hz, 1H, 4, 4′, 5, or 5′), 2.69 (br, 2H, C_2H_4), 2.27 (br, 2H, C_2H_4). $^{13}C\{^1H\}$ NMR (201 MHz, CD_2Cl_2): δ 151.9, 150.1, 148.5, 145.0, 134.5, 134.1, 132.9, 132.5, 131.9, 131.6, 131.5, 130.0, 128.9, 128.9, 128.6, 128.1, 128.3, 127.9, 122.1, 121.5, 117.5, 117.0, 102.9, 102.6, 50.3 (C_2H_4). Anal. Calcd for $C_{26}H_{20}N_4RhCl$: C, 59.28; H, 3.83; N, 10.63. Found: C, 59.28; H, 3.91; N, 10.41.

(5-^{NP}FP)Rh(Me)(X)(X′) (**3b**). Iodomethane (1 mL) was added dropwise to a THF solution (20 mL) of (5-^{NP}FP)Rh(Cl)(η^2-C_2H_4) (**3a**) (42 mg, 79 μmol) and stirred for 48 h. The reaction mixture was dried under vacuum. The resulting solid was dissolved in minimal amount of DCM, and pentane (30 mL) was added to the solution to give a yellow precipitate. The solid was collected by filtration, washed with pentane (3 × 10 mL), and dried under vacuum to afford a mixture of (5-^{NP}FP)Rh(Me)(X)(X′) (43 mg). The ^1H NMR spectrum is provided in Figure S25.

(5-^{NP}FP)Rh(Me)(TFA)$_2$ (**3c**).

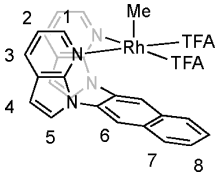

A THF solution (30 mL) of (5-^{NP}FP)Rh(Me)(X)(X′) (**3b**) (43 mg) was prepared, and AgTFA (30 mg, 135 μmol) was added to the solution, which was shielded from light using aluminum foil. After stirring for 24 h, the reaction mixture was filtered through Celite. The filtrate was dried under vacuum. The resulting solid was dissolved in minimal amount of DCM, and pentane (30 mL) was added to the solution to give a white precipitate. The solid was collected by filtration, washed with pentane (3 × 10 mL), and dried

https://doi.org/10.1021/acs.organomet.1c00223
Organometallics 2021, 40, 1889−1906

under vacuum to afford analytically pure (5-^{NP}FP)Rh(Me)$(TFA)_2$ (39 mg, yield = 81%). X-ray quality crystals of (5-^{NP}FP)Rh(Me)-$(TFA)_2$ (**3c**) were obtained by slow vapor diffusion of *n*-pentane into a solution of complex **3c** in THF. ^{1}H NMR (600 MHz, CD_2Cl_2): δ 8.33 (d, $^3J_{HH}$ = 6 Hz, 2H, 1), 8.26 (s, 2H, 6), 8.03 (dd, AA′BB′, $^3J_{HH}$ = 7, 5 Hz, 2H, 7 or 8), 7.90 (d, $^3J_{HH}$ = 8 Hz, 2H, 3), 7.79 (dd, AA′BB′, $^3J_{HH}$ = 7, 5 Hz, 2H, 7 or 8), 7.33 (d, $^3J_{HH}$ = 4 Hz, 2H, 4 or 5), 7.08 (dd, $^3J_{HH}$ = 8, 6 Hz, 2H, 2), 6.65 (d, $^3J_{HH}$ = 4 Hz, 2H, 4 or 5), 3.76 (d, $^1J_{RhH}$ = 2 Hz, 3H, CH_3). $^{13}C\{^1H\}$ NMR (201 MHz, CD_2Cl_2): δ 162.9 (q, $^2J_{CF}$ = 36 Hz, $COCF_3$), 153.5, 146.2, 134.9, 134.6, 132.4, 131.6, 129.9, 129.3, 129.2, 123.1, 118.0, 113.0 (q, $^2J_{CF}$ = 290 Hz, $COCF_3$), 104.7, 21.9 (d, $^2J_{CRh}$ = 29 Hz). ^{19}F NMR (564 MHz, CD_2Cl_2): δ −73.6. Anal. Calcd for $C_{29}H_{19}N_4O_4F_6Rh$: C, 49.45; H, 2.72; N, 7.95. Found: C, 48.79; H, 2.65; N, 7.67.

*6-^{NP}FP (8,8′-(2,3-naphthalene)diquinoline) (**4**).*

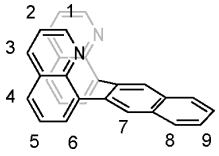

In a 500 mL pressure flask, 8-quinolineboronic acid (2.90 g, 16.8 mmol), 2,3-dibromonaphthalene (2.00 g, 7.0 mmol), Cs_2CO_3 (54 g, 168 mmol), and $Pd(PPh_3)_4$ (0.78 g, 0.7 mmol) were mixed in 120 mL of DMF in a glovebox. The pressure flask was capped, sealed, and heated at 120 °C for 24 h. The yellow mixture turned black after 15 h. After allowing the flask to cool to room temperature, the reaction mixture was filtered through a fine porosity frit loaded with Celite. Chloroform was used to wash the pressure flask and the frit, and the solutions were combined. Next, 100 mL of DI water was added to the solution, resulting in a bilayer mixture. The organic phase was separated and retained, and 200 mL of chloroform was added to extract the product from the aqueous layer (repeated twice). The extracted organic phases were combined and dried using sodium sulfate, and the solvent was removed under vacuum to give a brown oil. Benzene (100 mL) was added to dissolve the oil, and the solvent was removed under reduced pressure to give a brown sticky solid. Next, 300 mL of *n*-pentane was added, and solution was sonicated to facilitate the dispersal of solid in the mixture. Then, the solvent was again removed to give a yellow solid. This step was repeated until a pure white solid was obtained. The yellow solid was transferred to a fine porosity frit, and benzene (3 × 10 mL) was used to wash the product, resulting in an off-white solid. The solid was dissolved in minimal amount of DCM and then layered with hexanes to recrystallize. The colorless crystals were dissolved in DCM, and the solvent was removed. The solid was washed with *n*-pentane to obtain analytically pure 6-^{NP}FP (**4**) as a white powder. The isolated yield was 63%. X-ray quality crystals of 6-^{NP}FP (**4**) were obtained by bilayer diffusion using DCM and hexanes. ^{1}H NMR (800 MHz, C_6D_6): δ 8.65 (br, 2H, 1), 8.11 (s, 2H, 7), 7.76 (dd, AA′BB′, $^3J_{HH}$ = 7, 5 Hz, 2H, 8 or 9), 7.71 (br, 2H, 3), 7.38 (dd, $^3J_{HH}$ = 8 Hz, $^4J_{HH}$ = 2 Hz, 2H, 4 or 6), 7.31 (dd, AA′BB′, $^3J_{HH}$ = 7, 5 Hz, 2H, 8 or 9), 7.11 (d, $^3J_{HH}$ = 8 Hz, 2H, 4 or 6), 6.89 (dd, $^3J_{HH}$ = 8 Hz, 2H, 5), 6.68 (br, 2H, 2). $^{13}C\{^1H\}$ NMR (201 MHz, C_6D_6): δ 147.5, 145.4, 140.3, 137.0, 133.2, 131.0, 129.4, 128.5, 126.1, 126.1, 124.8, 123.8, 123.4, 118.3. Anal. Calcd for $C_{28}H_{18}N_2$: C, 87.93; H, 4.74; N, 7.32. Found: C, 87.31; H, 4.87; N, 7.11.

*(6-^{NP}FP)Rh(Cl)(η^2-C_2H_4) (**4a**).*

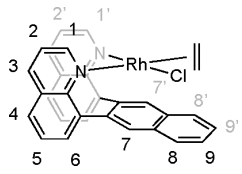

A THF solution (10 mL) of 6-^{NP}FP (**4**) (38 mg, 100 μmol) was added dropwise to a THF solution (30 mL) of $[Rh(\eta^2\text{-}C_2H_4)_2(\mu\text{-}Cl)]_2$ (19 mg, 50 μmol) and stirred for 24 h. The reaction mixture was dried under vacuum. The resulting solid was dissolved in minimal amount of DCM, and pentane (50 mL) was added to the solution to give a red precipitate. The solid was collected by filtration, washed with pentane (3 × 10 mL), and dried under vacuum to afford analytically pure (6-^{NP}FP)Rh(Cl)(η^2-C_2H_4) (39.5 mg, yield = 72%). ^{1}H NMR (600 MHz, CD_2Cl_2): δ 9.28 (dd, $^3J_{HH}$ = 5 Hz, $^4J_{HH}$ = 2 Hz, 1H, 1 or 1′), 8.45 (d, $^3J_{HH}$ = 7 Hz, 1H, 4 or 4′), 8.26 (d, $^3J_{HH}$ = 5 Hz, 1H, 1 or 1′), 8.07 (d, $^3J_{HH}$ = 8 Hz, 1H, 3 or 3′), 7.97 (d, $^3J_{HH}$ = 8 Hz, 1H, 3 or 3′), 7.89 (d, $^3J_{HH}$ = 8 Hz, 1H, 4 or 4′), 7.80 (d, $^3J_{HH}$ = 8 Hz, 1H, 8, 8′, 9, or 9′), 7.76 (d, $^3J_{HH}$ = 8 Hz, 1H, 8, 8′, 9, or 9′), 7.73 (d, $^3J_{HH}$ = 8 Hz, 1H, 8, 8′, 9, or 9′), 7.69 (s, 1H, 7 or 7′), 7.44 (dd, $^3J_{HH}$ = 7 Hz, 1H, 5 or 5′), 7.40 (dd, ^{3}JHH = 7 Hz, 1H, 5 or 5′), 7.34−7.31 (m, 2H, 2 or 2′; 8, 8′, 9, or 9′), 7.30 (s, 1H, 7 or 7′), 7.20 (d, $^3J_{HH}$ = 7 Hz, 1H, 6 or 6′), 7.11 (d, 3JHH = 8 Hz, 1H, 6 or 6′), 7.09 (dd, $^3J_{HH}$ = 4 Hz, 1H, 2 or 2′), 4.00 (t, $^3J_{HH}$ = 10 Hz, 1H, C_2H_4), 3.81 (t, $^3J_{HH}$ = 10 Hz, 1H, C_2H_4), 3.28 (t, $^3J_{HH}$ = 10 Hz, 1H, C_2H_4), 2.69 (t, $^3J_{HH}$ = 10 Hz, 1H, C_2H_4). $^{13}C\{^1H\}$ NMR (201 MHz, CD_2Cl_2): δ 158.0, 152.7, 149. 8, 142.3, 142.1, 140.4, 138.4, 136.0, 135.9, 135.1, 132.2, 131.5, 130.7, 123.0, 129.5, 129.3, 128.1, 127.9, 127.8, 127.6, 127.5, 126.9, 125.7, 125.3, 122.5, 121.5, 98.3 (d, $^1J_{CRh}$ = 3 Hz), 90.2 (d, $^1J_{CRh}$ = 6 Hz), 51.0 (d, $^1J_{CRh}$ = 15 Hz, C_2H_4), 45.1 (d, $^1J_{CRh}$ = 15 Hz, C_2H_4). Acceptable elemental analysis results for **4a** could not be obtained. The NMR spectra of **4a** appear in Figures S34−S37.

*(6-^{NP}FP)Rh(Me)(X)(X′) (**4b**).* Iodomethane (1 mL) was added dropwise to a THF solution (20 mL) of (6-^{NP}FP)Rh(Cl)(η^2-C_2H_4) (**4a**) (39.5 mg, 72 μmol) and stirred for 24 h. The reaction mixture was dried under vacuum. The resulting solid was dissolved in minimal amount of DCM, and pentane (30 mL) was added to the solution to give a yellow precipitate. The solid was collected by filtration, washed with pentane (3 × 10 mL), and dried under vacuum to afford a mixture of (6-^{NP}FP)Rh(Me)(X)(X′) (35.0 mg). The ^{1}H NMR spectrum is provided in Figure S38.

*(6-^{NP}FP)Rh(Me)$(TFA)_2$ (**4c**).*

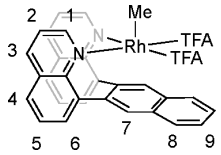

A THF solution (60 mL) of (6-^{NP}FP)Rh(Me)(X)(X′) (**4b**) (192 mg) was prepared, and AgTFA (128 mg, 579 μmol) was added to the solution, which was shielded from light using aluminum foil. After stirring for 24 h, the reaction mixture was filtered through Celite. The filtrate was dried under vacuum. The resulting solid was dissolved in minimal amount of DCM (5 mL), and pentane (50 mL) was added to the solution to give a white precipitate. The solid was collected by filtration, washed with pentane (3 × 10 mL), and dried under vacuum to afford analytically pure (6-^{NP}FP)Rh(Me)$(TFA)_2$ (121 mg, yield = 58%). X-ray quality crystals of (6-^{NP}FP)Rh(Me)-$(TFA)_2$ (**4c**) were obtained by slow vapor diffusion of *n*-pentane into a solution of complex **4c** in THF. ^{1}H NMR (600 MHz, CD_2Cl_2): δ 8.82 (d, $^3J_{HH}$ = 6 Hz, 2H, 1), 8.27 (s, 2H, 7), 8.17 (dd, $^3J_{HH}$ = 8 Hz, $^4J_{HH}$ = 2 Hz, 2H, 3), 7.98 (dd, AA′BB′, $^3J_{HH}$ = 7, 5 Hz, 8 or 9), 7.70 (dd, $^3J_{HH}$ = 8 Hz, $^4J_{HH}$ = 1 Hz, 2H, 4 or 6), 7.67 (dd, AA′BB′, $^3J_{HH}$ = 7, 5 Hz, 2H, 8 or 9), 7.61 (dd, $^3J_{HH}$ = 7 Hz, $^4J_{HH}$ = 1 Hz, 2H, 4 or 6), 7.49 (dd, $^3J_{HH}$ = 8, 7 Hz, 2H, 5), 7.32 (dd, $^3J_{HH}$ = 8, 5 Hz, 2H, 2), 3.20 (d, $^2J_{RhH}$ = 2 Hz, 3H, CH_3). $^{13}C\{^1H\}$ NMR (201 MHz, CD_2Cl_2): δ 162.7 (q, $^2J_{FC}$ = 36 Hz, $COCF_3$), 156.7, 151.2, 139.9, 137.9, 136.5, 134.6, 134.5, 129.9, 129.4, 129.0, 129.0, 128.6, 122.2, 114.5 (q, $^1J_{FC}$ = 292 Hz, $COCF_3$), 23.9 (d, $^1J_{RhC}$ = 27 Hz, $RhCH_3$). ^{19}F NMR (564 MHz, CD_2Cl_2): δ −73.7. Anal. Calcd for $C_{33}H_{21}N_2O_4F_6Rh$: C, 54.56; H, 2.91; N, 3.86. Found: C, 53.74; H, 2.99; N, 3.77.

*(dpe)Rh(Me)$(TFA)_2$ (**5c**).* A diethyl ether (10 mL) suspension of 1,2-dpe (119 mg, 646 μmol) was added dropwise into a diethyl ether (30 mL) suspension of $[Rh(\eta^2\text{-}C_2H_4)_2(\mu\text{-}Cl)]_2$ (126 mg, 323 μmol) in a round-bottomed flask, resulting in a change in color of the suspension from orange to yellow and ultimately to red. The reaction mixture was allowed to stir for 4 h, and then MeI (0.5 mL) was

https://doi.org/10.1021/acs.organomet.1c00223
Organometallics 2021, 40, 1889−1906

added dropwise, turning the yellow suspension to a brown suspension. The reaction mixture was allowed to stir for 1 day, and cold *n*-pentane (−30 °C, 30 mL) was added. The solid was collected by filtration, washed with pentane (3 × 10 mL), and dried under vacuum for 2 h. Then, the solid was suspended in THF (30 mL), and AgTFA (145 mg, 657 μmol) was added into the mixture, which was shielded from light using aluminum foil. After stirring for 24 h, the reaction mixture was filtered through Celite. The filtrate was dried under vacuum. The resulting solid was dissolved in minimal amount of DCM (~5 mL), and cold *n*-pentane (−30 °C, 50 mL) was added to the solution to give a pale-yellow precipitate. The solid was collected by filtration, washed with pentane (3 × 10 mL), and dried under vacuum. Recrystallization through slow vapor diffusion of *n*-pentane into a solution in THF afforded analytically pure (dpe)Rh(Me)$(TFA)_2$ (286 mg, yield = 84%). X-ray quality crystals of (dpe)Rh(Me)$(TFA)_2$ (**5c**) were obtained by the same method as described for recrystallization. ^{1}H NMR (600 MHz, CD_2Cl_2): δ 8.16 (d, $^3J_{HH}$ = 6 Hz, 1H, py), 7.74 (dd, $^3J_{HH}$ = 8 Hz, 1H, py), 7.33 (d, $^3J_{HH}$ = 8 Hz, 1H, py), 7.23 (dd, $^3J_{HH}$ = 7 Hz, 1H, py), 4.88−4.79 (m, 1H, CH_2CH_2), 3.75−3.66 (m, 1H, CH_2CH_2), 3.44 (d, $^2J_{HRh}$ = 3 Hz, 1H, Me). $^{13}C\{^1H\}$ NMR (201 MHz, CD_2Cl_2): δ 164.6, 164.0 (q, $^2J_{CF}$ = 37 Hz, $COCF_3$), 151.1, 138.6, 126.0, 123.7, 114.2 (q, $^1J_{CF}$ = 290 Hz, $COCF_3$), 33.8, 19.5 (d, $^1J_{CRh}$ = 32 Hz). ^{19}F NMR (564 MHz, CD_2Cl_2): δ −73.7. Anal. Calcd for $C_{17}H_{15}N_2O_4F_6Rh$: C, 38.66; H, 2.86; N, 5.30. Found: C, 38.49; H, 2.72; N, 5.09.

NMR Study of Reductive Elimination. In a J. Young tube equipped with a sealed capillary containing a CD_3CN solution of hexamethyldisiloxane (HMDSO), 0.01 M (with exceptions when there is solubility issue) solutions of the Rh^{III}−Me complex (**1c**, **2c**, **3c**, **4c**, and **5c**) were made in deuterated solvent (5 mL) inside the glovebox. A starting ^{1}H NMR spectrum was recorded. The J. Young tube was then charged with 30 psig N_2 and heated in oil bath. After each time period, the J. Young tube was removed from the oil bath and allowed to cool to room temperature, and a ^{1}H NMR spectrum was acquired. The yield of MeX was calculated using the integration of MeX peaks relative to HMDSO divided by the integration of Rh−Me relative to HMDSO in the starting ^{1}H NMR spectrum.

Computational Methods. All DFT quantum chemical calculations were performed using the Jaguar software package version 8.4 from Schrodinger Inc. Structures were optimized using the B3LYP flavor of DFT with the Grimmie−Becke−Johnson D3 correction for London dispersion forces. For the initial vacuum calculations, the organic elements were described using the 6-31G* basis set while Rh and Ag were treated with the Los Alamos large-core pseudopotential (leaving 9 explicit electrons on Rh and 11 on Ag). After vacuum optimizations, the structures were reoptimized at the B3LYP-D3 level with the LACV3P**++ basis set, which treats organics with the 6-311G**++ basis set and describes Rh and Ag with a small core pseudopotential (17 explicit electrons on Rh and 19 on Ag). Additionally, solvent effects were applied using the PBF Poisson−Boltzmann implicit solvation model to describe the medium outside the solvent accessible surface. To mimic the CD_3CN solvent environment, we chose a dielectric constant of 37.5 and calculated a probe radius of 2.19 A according to the equation $r = \sqrt[3]{3\Delta MW/4\pi N_A\rho}$ where Δ is the liquid packing density, MW is the molecular weight, N_A is Avogadro's number, and ρ is the density. After these solvent optimizations, we calculated the vibrational frequencies to confirm local minima for stationary geometries and saddle points for transition states and to obtain thermochemical properties at 423 K.

Crystallographic Details. A suitable single crystal of each sample was coated with Paratone oil and mounted on a MiTeGen MicroLoop. The X-ray intensity data were measured on a Bruker Kappa APEXII Duo system. An Incoatec Microfocus IμS (Cu Kα, λ = 1.54178 Å) and a multilayer mirror monochromator were used for **1c** and **4c**. A fine-focus sealed tube (Mo Kα, λ = 0.71073 Å) and a graphite monochromator were used for all other crystals. The frames were integrated with the Bruker SAINT software package[78] using a narrow-frame algorithm. Data were corrected for absorption effects using the Multi-Scan method (SADABS).[78] Each structure was solved and refined using the Bruker SHELXTL Software Package[79] within APEX3[78] and OLEX2.[80] Non-hydrogen atoms were refined anisotropically. In **1a**, **2a**, and **3a**, the ethylene hydrogen atoms were located and refined isotropically with U_{iso} = 1.2U_{equiv} of the parent C atoms. All other hydrogen atoms in all structures were placed in geometrically calculated positions with U_{iso} = 1.2U_{equiv} of the parent atom (U_{iso} = 1.5U_{equiv} for methyl). In **1a**, two solvent sites were identified in the asymmetric unit. One contained a well-behaved THF solvent molecule, and the other was severely disordered and could not be adequately modeled with or without restraints. Thus, the structure factors were modified using the PLATON SQUEEZE[81] technique, in order to produce a "solvate-free" structure factor set. PLATON reported a total electron density of 119 e^- and a total solvent accessible volume of 536 $Å^3$. In **4c**, the symmetry-disordered sites were refined at half-occupancy to satisfy the symmetry requirements. Portions of **1c**, **2c**, **3c**, and **4c** were disordered over two positions. The relative occupancies of each disordered fragment were freely refined. Constraints were used on the anisotropic displacement parameters of most of the disordered atoms and restraints were used on most disordered bonds. In **5c**, the symmetry-disordered THF solvent molecule was refined at half-occupancy with restraints on its anisotropic displacement parameters.

■ ASSOCIATED CONTENT

Supporting Information

The Supporting Information is available free of charge at https://pubs.acs.org/doi/10.1021/acs.organomet.1c00223.

Additional experimental details, NMR spectra of the compounds and the reactions, cyclic voltammetry, DFT-optimized structures, and crystal structure data- (PDF)

DFT-optimized coordinates (XYZ)

Accession Codes

CCDC 2046421−2046427, 2046429−2046432, and 2068537 contains the supplementary crystallographic data for this paper. These data can be obtained free of charge via www.ccdc.cam.ac.uk/data_request/cif, or by emailing data_request@ccdc.cam.ac.uk, or by contacting The Cambridge Crystallographic Data Centre, 12 Union Road, Cambridge CB2 1EZ, UK; fax: +44 1223 336033.

■ AUTHOR INFORMATION

Corresponding Authors

T. Brent Gunnoe − *Department of Chemistry, University of Virginia, Charlottesville, Virginia 22904, United States;* orcid.org/0000-0001-5714-3887; Email: tbg7h@virginia.edu

William A. Goddard III − *Materials and Process Simulation Center, California Institute of Technology, Pasadena, California 91125, United States;* orcid.org/0000-0003-0097-5716; Email: wag@ caltech.edu

Authors

Shunyan Gu − *Department of Chemistry, University of Virginia, Charlottesville, Virginia 22904, United States;* orcid.org/0000-0002-3625-1042

Junqi Chen − *Department of Chemistry, University of Virginia, Charlottesville, Virginia 22904, United States*

Charles B. Musgrave III − *Materials and Process Simulation Center, California Institute of Technology, Pasadena, California 91125, United States;* orcid.org/0000-0002-3432-0817

https://doi.org/10.1021/acs.organomet.1c00223
Organometallics 2021, 40, 1889−1906

Zoë M. Gehman − *Department of Chemistry, University of Virginia, Charlottesville, Virginia 22904, United States*
Laurel G. Habgood − *Department of Chemistry, Rollins College, Winter Park, Florida 32789, United States*
Xiaofan Jia − *Department of Chemistry, University of Virginia, Charlottesville, Virginia 22904, United States;* orcid.org/0000-0003-0425-5089
Diane A. Dickie − *Department of Chemistry, University of Virginia, Charlottesville, Virginia 22904, United States;* orcid.org/0000-0003-0939-3309

Complete contact information is available at: https://pubs.acs.org/10.1021/acs.organomet.1c00223

Author Contributions

#S.G. and J.C. contributed equally to this work.

Notes

The authors declare no competing financial interest.

■ ACKNOWLEDGMENTS

The Gunnoe group acknowledges support from the U.S. National Science Foundation (1800173). C.B.M. and W.A.G. acknowledge support from the NSF (CBET-1805022). Single-crystal X-ray diffraction experiments were performed on a diffractometer at the University of Virginia funded by the NSF-MRI program (CHE-2018870).

■ REFERENCES

(1) Conley, B. L.; Tenn, W. J., III; Young, K. J. H.; Ganesh, S.; Meier, S.; Ziatdinov, V.; Mironov, O.; Oxgaard, J.; Gonzales, J.; Goddard, W. A., III; Periana, R. A. Methane Functionalization. In *Activation of Small Molecules*; Tolman, W. B., Ed.; Wiley-VCH Verlag GmbH & Co.: Weinheim, 2006.
(2) Hartwig, J. F. *Organotransition Metal Chemistry: From Bonding to Catalysis*; University Science Books, 2010.
(3) Gunsalus, N. J.; Koppaka, A.; Park, S. H.; Bischof, S. M.; Hashiguchi, B. G.; Periana, R. A. Homogeneous Functionalization of Methane. *Chem. Rev.* **2017**, *117*, 8521−8573.
(4) Shilov, A. E.; Shul'pin, G. B. Activation of C−H bonds by metal complexes. *Chem. Rev.* **1997**, *97*, 2879−2932.
(5) Caballero, A.; Pérez, P. J. Methane as raw material in synthetic chemistry: The final frontier. *Chem. Soc. Rev.* **2013**, *42*, 8809−8820.
(6) Goldberg, K. I.; Goldman, A. S. Large-scale selective functionalization of alkanes. *Acc. Chem. Res.* **2017**, *50*, 620−626.
(7) Arndtsen, B. A.; Bergman, R. G.; Mobley, T. A.; Peterson, T. H. Selective Intermolecular Carbon-Hydrogen Bond Activation by Synthetic Metal Complexes in Homogeneous Solution. *Acc. Chem. Res.* **1995**, *28*, 154−162.
(8) Jones, W. D.; Feher, F. J. Comparative reactivities of hydrocarbon carbon-hydrogen bonds with a transition-metal complex. *Acc. Chem. Res.* **1989**, *22*, 91−100.
(9) Webb, J. R.; Bolaño, T.; Gunnoe, T. B. Catalytic Oxy-Functionalization of Methane and Other Hydrocarbons: Fundamental Advancements and New Strategies. *ChemSusChem* **2011**, *4*, 37−49.
(10) Labinger, J. A.; Bercaw, J. E. Understanding and exploiting C−H bond activation. *Nature* **2002**, *417*, 507−514.
(11) Olah, G. A.; Molnár, Á. *Hydrocarbon Chemistry*; John Wiley & Sons, 2003.
(12) Periana, R. A.; Bhalla, G.; Tenn, W. J.; Young, K. J. H.; Liu, X. Y.; Mironov, O.; Jones, C. J.; Ziatdinov, V. R. Perspectives on some challenges and approaches for developing the next generation of selective, low temperature, oxidation catalysts for alkane hydroxylation based on the CH activation reaction. *J. Mol. Catal. A: Chem.* **2004**, *220*, 7−25.
(13) Labinger, J. A. Selective alkane oxidation: hot and cold approaches to a hot problem. *J. Mol. Catal. A: Chem.* **2004**, *220*, 27−35.
(14) Gol'dshleger, N. F.; Tyabin, M. B.; Shilov, A. E.; Shteinman, A. A. Activation of Saturated Hydrocarbons-Deuterium-Hydrogen Exchange in Solutions of Transition Metal Complexes. *Russ. J. Phys. Chem.* **1969**, *43*, 1222−1223.
(15) Gol'dshleger, N. F.; Shteinma, A. A.; Shilov, A. E.; Eskova, V. V. Reactions of alkanes in solutions of chloride complexes of platinum. *Russ. J. Phys. Chem.* **1972**, *46*, 785−786.
(16) Muehlhofer, M.; Strassner, T.; Herrmann, W. A. New catalyst systems for the catalytic conversion of methane into methanol. *Angew. Chem., Int. Ed.* **2002**, *41*, 1745−1747.
(17) Hashiguchi, B. G.; Konnick, M. M.; Bischof, S. M.; Gustafson, S. J.; Devarajan, D.; Gunsalus, N.; Ess, D. H.; Periana, R. A. Main-Group Compounds Selectively Oxidize Mixtures of Methane, Ethane, and Propane to Alcohol Esters. *Science* **2014**, *343*, 1232−1237.
(18) Lin, M.; Sen, A. Direct catalytic conversion of methane to acetic acid in an aqueous medium. *Nature* **1994**, *368*, 613−615.
(19) Wong-Foy, A. G.; Bhalla, G.; Liu, X. Y.; Periana, R. A. Alkane C−H Activation and Catalysis by an O-Donor Ligated Iridium Complex. *J. Am. Chem. Soc.* **2003**, *125*, 14292−14293.
(20) Periana, R. A.; Taube, D. J.; Evitt, E. R.; Löffler, D. G.; Wentrcek, P. R.; Voss, G.; Masuda, T. A mercury-catalyzed, high-yield system for the oxidation of methane to methanol. *Science* **1993**, *259*, 340−343.
(21) Periana, R. A.; Taube, D. J.; Gamble, S.; Taube, H.; Satoh, T.; Fujii, H. Platinum catalysts for the high-yield oxidation of methane to a methanol derivative. *Science* **1998**, *280*, 560−564.
(22) Stahl, S. S.; Labinger, J. A.; Bercaw, J. E. Homogeneous oxidation of alkanes by electrophilic late transition metals. *Angew. Chem., Int. Ed.* **1998**, *37*, 2180−2192.
(23) Jones, C. J.; Taube, D.; Ziatdinov, V. R.; Periana, R. A.; Nielsen, R. J.; Oxgaard, J.; Goddard, W. A., III Selective Oxidation of Methane to Methanol Catalyzed, with C−H Activation, by Homogeneous, Cationic Gold. *Angew. Chem., Int. Ed.* **2004**, *43*, 4626−4629.
(24) Gretz, E.; Oliver, T. F.; Sen, A. Carbon-hydrogen bond activation by electrophilic transition-metal compounds. Palladium-(II)-mediated oxidation of arenes and alkanes including methane. *J. Am. Chem. Soc.* **1987**, *109*, 8109−8111.
(25) Mironov, O. A.; Bischof, S. M.; Konnick, M. M.; Hashiguchi, B. G.; Ziatdinov, V. R.; Goddard, W. A.; Ahlquist, M.; Periana, R. A. Using Reduced Catalysts for Oxidation Reactions: Mechanistic Studies of the "Periana-Catalytica" System for CH4 Oxidation. *J. Am. Chem. Soc.* **2013**, *135*, 14644−14658.
(26) Tenn, W. J.; Young, K. J. H.; Bhalla, G.; Oxgaard, J.; Goddard, W. A., III; Periana, R. A. CH Activation with an O-Donor Iridium−Methoxo Complex. *J. Am. Chem. Soc.* **2005**, *127*, 14172−14173.
(27) Luinstra, G. A.; Wang, L.; Stahl, S. S.; Labinger, J. A.; Bercaw, J. E. C−H activation by aqueous platinum complexes: A mechanistic study. *J. Organomet. Chem.* **1995**, *504*, 75−91.
(28) Luinstra, G. A.; Labinger, J. A.; Bercaw, J. E. Mechanism and stereochemistry for nucleophilic attack at carbon of platinum (IV) alkyls: Model reactions for hydrocarbon oxidation with aqueous platinum chlorides. *J. Am. Chem. Soc.* **1993**, *115*, 3004−3005.
(29) Kloek, S. M.; Heinekey, D. M.; Goldberg, K. I. C−H Bond Activation by Rhodium(I) Hydroxide and Phenoxide Complexes. *Angew. Chem., Int. Ed.* **2007**, *46*, 4736−4738.
(30) Janowicz, A. H.; Bergman, R. G. Carbon-hydrogen activation in completely saturated hydrocarbons: direct observation of M + R-H → M(R)(H). *J. Am. Chem. Soc.* **1982**, *104*, 352−354.
(31) Vaughan, B. A.; Webster-Gardiner, M. S.; Cundari, T. R.; Gunnoe, T. B. A rhodium catalyst for single-step styrene production from benzene and ethylene. *Science* **2015**, *348*, 421−424.
(32) Gunnoe, T. B. Metal-Mediated Carbon-Hydrogen Bond Activation. In *Physical Inorganic Chemistry: Reactions, Processes, and Applications*; Bakac, A., Ed.; Wiley, 2010; pp 495−550.

(33) Colby, D. A.; Tsai, A. S.; Bergman, R. G.; Ellman, J. A. Rhodium Catalyzed Chelation-Assisted C−H Bond Functionalization Reactions. *Acc. Chem. Res.* **2012**, *45*, 814−825.
(34) Piou, T.; Rovis, T. Electronic and Steric Tuning of a Prototypical Piano Stool Complex: Rh(III) Catalysis for C−H Functionalization. *Acc. Chem. Res.* **2018**, *51*, 170−180.
(35) Gensch, T.; Hopkinson, M. N.; Glorius, F.; Wencel-Delord, J. Mild metal-catalyzed C−H activation: examples and concepts. *Chem. Soc. Rev.* **2016**, *45*, 2900−2936.
(36) Jones, W. D.; Feher, F. J. Alkane carbon-hydrogen bond activation by homogeneous rhodium(I) compounds. *Organometallics* **1983**, *2*, 562−563.
(37) Jones, W. D. On the Nature of Carbon−Hydrogen Bond Activation at Rhodium and Related Reactions. *Inorg. Chem.* **2005**, *44*, 4475−4484.
(38) Colby, D. A.; Bergman, R. G.; Ellman, J. A. Rhodium-Catalyzed C−C Bond Formation via Heteroatom-Directed C−H Bond Activation. *Chem. Rev.* **2010**, *110*, 624−655.
(39) Periana, R. A.; Bergman, R. G. Isomerization of the hydridoalkylrhodium complexes formed on oxidative addition of rhodium to alkane carbon-hydrogen bonds. Evidence for the intermediacy of.eta.2-alkane complexes. *J. Am. Chem. Soc.* **1986**, *108*, 7332−7346.
(40) Webster-Gardiner, M. S.; Fu, R.; Fortman, G. C.; Nielsen, R. J.; Gunnoe, T. B.; Goddard, W. A., III Arene C−H activation using Rh(I) catalysts supported by bidentate nitrogen chelates. *Catal. Sci. Technol.* **2015**, *5*, 96−100.
(41) Webster-Gardiner, M. S.; Piszel, P. E.; Fu, R.; McKeown, B. A.; Nielsen, R. J.; Goddard, W. A., III; Gunnoe, T. B. Electrophilic RhI catalysts for arene H/D exchange in acidic media: Evidence for an electrophilic aromatic substitution mechanism. *J. Mol. Catal. A: Chem.* **2017**, *426*, 381−388.
(42) Webster-Gardiner, M. S.; Chen, J.; Vaughan, B. A.; McKeown, B. A.; Schinski, W.; Gunnoe, T. B. Catalytic Synthesis of "Super" Linear Alkenyl Arenes Using an Easily Prepared Rh(I) Catalyst. *J. Am. Chem. Soc.* **2017**, *139*, 5474−5480.
(43) Vaughan, B. A.; Khani, S. K.; Gary, J. B.; Kammert, J. D.; Webster-Gardiner, M. S.; McKeown, B. A.; Davis, R. J.; Cundari, T. R.; Gunnoe, T. B. Mechanistic Studies of Single-Step Styrene Production Using a Rhodium(I) Catalyst. *J. Am. Chem. Soc.* **2017**, *139*, 1485−1498.
(44) Chen, J.; Nielsen, R. J.; Goddard, W. A., III; McKeown, B. A.; Dickie, D. A.; Gunnoe, T. B. Catalytic Synthesis of Superlinear Alkenyl Arenes Using a Rh(I) Catalyst Supported by a "Capping Arene" Ligand: Access to Aerobic Catalysis. *J. Am. Chem. Soc.* **2018**, *140*, 17007−17018.
(45) Zhu, W.; Luo, Z.; Chen, J.; Liu, C.; Yang, L.; Dickie, D. A.; Liu, N.; Zhang, S.; Davis, R. J.; Gunnoe, T. B. Mechanistic Studies of Single-Step Styrene Production Catalyzed by Rh Complexes with Diimine Ligands: An Evaluation of the Role of Ligands and Induction Period. *ACS Catal.* **2019**, *9*, 7457−7475.
(46) Zhu, W.; Gunnoe, T. B. Advances in Rhodium-Catalyzed Oxidative Arene Alkenylation. *Acc. Chem. Res.* **2020**, *53*, 920−936.
(47) Jia, X.; Frye, L. I.; Zhu, W.; Gu, S.; Gunnoe, T. B. Synthesis of Stilbenes by Rhodium-Catalyzed Aerobic Alkenylation of Arenes via C−H Activation. *J. Am. Chem. Soc.* **2020**, *142*, 10534−10543.
(48) Gu, S.; Nielsen, R. J.; Taylor, K. H.; Fortman, G. C.; Chen, J.; Dickie, D. A.; Goddard, W. A.; Gunnoe, T. B. Use of Ligand Steric Properties to Control the Thermodynamics and Kinetics of Oxidative Addition and Reductive Elimination with Pincer-Ligated Rh Complexes. *Organometallics* **2020**, *39*, 1917−1933.
(49) Kong, F.; Gu, S.; Liu, C.; Dickie, D. A.; Zhang, S.; Gunnoe, T. B. Effects of Additives on Catalytic Arene C−H Activation: Study of Rh Catalysts Supported by Bis-phosphine Pincer Ligands. *Organometallics* **2020**, *39*, 3918−3935.
(50) Frech, C. M.; Milstein, D. Direct Observation of Reductive Elimination of Methyl Iodide from a Rhodium(III) Pincer Complex: The Importance of Sterics. *J. Am. Chem. Soc.* **2006**, *128*, 12434−12435.
(51) Feller, M.; Iron, M. A.; Shimon, L. J. W.; Diskin-Posner, Y.; Leitus, G.; Milstein, D. Competitive C−I versus C−CN Reductive Elimination from a Rh^{III} Complex. Selectivity is Controlled by the Solvent. *J. Am. Chem. Soc.* **2008**, *130*, 14374−14375.
(52) Feller, M.; Diskin-Posner, Y.; Leitus, G.; Shimon, L. J. W.; Milstein, D. Direct Observation of Reductive Elimination of MeX (X = Cl, Br, I) from Rh^{III} Complexes: Mechanistic Insight and the Importance of Sterics. *J. Am. Chem. Soc.* **2013**, *135*, 11040−11047.
(53) O'Reilly, M. E.; Pahls, D. R.; Webb, J. R.; Boaz, N. C.; Majumdar, S.; Hoff, C. D.; Groves, J. T.; Cundari, T. R.; Gunnoe, T. B. Reductive functionalization of a rhodium(III)−methyl bond by electronic modification of the supporting ligand. *Dalton Trans* **2014**, *43*, 8273−8281.
(54) O'Reilly, M. E.; Pahls, D. R.; Cundari, T. R.; Gunnoe, T. B. Reductive Functionalization of a Rhodium(III)−Methyl Bond in Acidic Media: Key Step in the Electrophilic Functionalization of Methane. *Organometallics* **2014**, *33*, 6504−6510.
(55) Bianchini, C.; Meli, A.; Peruzzini, M.; Ramirez, J. A.; Vacca, A.; Vizza, F.; Zanobini, F. Oxidative addition/reductive elimination of aldehydes and ketones at rhodium. *Organometallics* **1989**, *8*, 337−345.
(56) Milstein, D. The first isolated, stable cis-hydridoalkylrhodium complexes and their reductive elimination reaction. *J. Am. Chem. Soc.* **1982**, *104*, 5227−5228.
(57) Pedersen, A.; Tilset, M. Oxidatively induced reductive eliminations. Kinetics and mechanism of the elimination of ethane from the 17-electron cation radical of rhodium complex Cp*Rh-$(PPh_3)(CH_3)_2$. *Organometallics* **1993**, *12*, 56−64.
(58) Kim, J.; Shin, K.; Jin, S.; Kim, D.; Chang, S. Oxidatively Induced Reductive Elimination: Exploring the Scope and Catalyst Systems with Ir, Rh, and Ru Complexes. *J. Am. Chem. Soc.* **2019**, *141*, 4137−4146.
(59) O'Reilly, M. E.; Johnson, S. I.; Nielsen, R. J.; Goddard, W. A.; Gunnoe, T. B. Transition-Metal-Mediated Nucleophilic Aromatic Substitution with Acids. *Organometallics* **2016**, *35*, 2053−2056.
(60) O'Reilly, M. E.; Fu, R.; Nielsen, R. J.; Sabat, M.; Goddard, W. A.; Gunnoe, T. B. Long-Range C−H Bond Activation by Rh^{III}-Carboxylates. *J. Am. Chem. Soc.* **2014**, *136*, 14690−14693.
(61) Fu, R.; O'Reilly, M. E.; Nielsen, R. J.; Goddard, W. A., III; Gunnoe, T. B. Rhodium Bis(quinolinyl)benzene Complexes for Methane Activation and Functionalization. *Chem. - Eur. J.* **2015**, *21*, 1286−1293.
(62) Tan, R.; Jia, P.; Rao, Y.; Jia, W.; Hadzovic, A.; Yu, Q.; Li, X.; Song, D. Diplatinum Complexes Supported by Novel Tetradentate Ligands with Quinoline Functionalities for Tandem C−Cl Activation and Dearomatization. *Organometallics* **2008**, *27*, 6614−6622.
(63) Zhao, S.-B.; Song, D.; Jia, W.-L.; Wang, S. Regioselective C−H Activation of Toluene with a 1,2-Bis(*N*-7-azaindolyl)benzene Platinum(II) Complex. *Organometallics* **2005**, *24*, 3290−3296.
(64) Stumpf, T.-D. J.; Steinbach, M.; Hölтke, M.; Heuger, G.; Grasemann, F.; Fröhlich, R.; Schindler, S.; Göttlich, R. C-Bridged Bispyrrolidines and Bispiperidines as New Ligands. *Eur. J. Org. Chem.* **2018**, *2018*, 5538−5547.
(65) Liu, Z.; Yamamichi, H.; Madrahimov, S. T.; Hartwig, J. F. Rhodium Phosphine−π-Arene Intermediates in the Hydroamination of Alkenes. *J. Am. Chem. Soc.* **2011**, *133*, 2772−2782.
(66) Geier, S. J.; Chapman, E. E.; McIsaac, D. I.; Vogels, C. M.; Decken, A.; Westcott, S. A. Bulky rhodium diimine complexes for the catalyzed borylation of vinylarenes. *Inorg. Chem. Commun.* **2006**, *9*, 788−791.
(67) Kanas, D. A.; Geier, S. J.; Vogels, C. M.; Decken, A.; Westcott, S. A. Synthesis, Characterization, and Reactivity of Rhodium(I) Acetylacetonato Complexes Containing Pyridinecarboxaldimine Ligands. *Inorg. Chem.* **2008**, *47*, 8727−8735.
(68) Budzelaar, P. H. M.; Moonen, N. N. P.; de Gelder, R.; Smits, J. M. M.; Gal, A. W. Steric Control over Arene Coordination to β-Diiminate Rhodium(I) Fragments. *Chem. - Eur. J.* **2000**, *6*, 2740−2747.

https://doi.org/10.1021/acs.organomet.1c00223
Organometallics 2021, 40, 1889−1906

(69) Harman, W. D. The Activation of Aromatic Molecules with Pentaammineosmium(II). *Chem. Rev.* **1997**, *97*, 1953−1978.
(70) Liebov, B. K.; Harman, W. D. Group 6 Dihapto-Coordinate Dearomatization Agents for Organic Synthesis. *Chem. Rev.* **2017**, *117*, 13721−13755.
(71) Lau, W.; Huffman, J. C.; Kochi, J. K. Electrochemical oxidation-reduction of organometallic complexes. Effect of the oxidation state on the pathways for reductive elimination of dialkyliron complexes. *Organometallics* **1982**, *1*, 155−169.
(72) Koo, K.; Hillhouse, G. L. Carbon-Nitrogen Bond Formation by Reductive Elimination from Nickel(II) Amido Alkyl Complexes. *Organometallics* **1995**, *14*, 4421−4423.
(73) Komiya, S.; Albright, T. A.; Hoffmann, R.; Kochi, J. K. The stability of organogold compounds. Hydrolytic, thermal, and oxidative cleavages of dimethylaurate(I) and tetramethylaurate(III). *J. Am. Chem. Soc.* **1977**, *99*, 8440−8447.
(74) Shin, K.; Park, Y.; Baik, M.-H.; Chang, S. Iridium-catalysed arylation of C−H bonds enabled by oxidatively induced reductive elimination. *Nat. Chem.* **2018**, *10*, 218−224.
(75) Huang, L.-a.; Shin, H.; Goddard, W. A.; Wang, J. Photochemically deposited Ir-doped NiCo oxyhydroxide nanosheets provide highly efficient and stable electrocatalysts for the oxygen evolution reaction. *Nano Energy* **2020**, *75*, 104885.
(76) Arndtsen, B. A.; Bergman, R. G. Unusually Mild and Selective Hydrocarbon C-H Bond Activation with Positively Charged Iridium(III) Complexes. *Science* **1995**, *270*, 1970.
(77) Cramer, R.; McCleverty, J. A.; Bray, J. Di-μ-chlorotetrakis-(ethylene)dirhodium(I), 2,4-Pentanedionatobis(ethylene)rhodium-(I), and Di-μ-chlorotetracarbonyldirhodium(I). *Inorg. Synth.* **1974**, *20*, 14.
(78) *Bruker Saint; SADABS; APEX3*; Bruker AXS Inc.: Madison, WI, 2012.
(79) Sheldrick, G. SHELXT - Integrated space-group and crystal-structure determination. *Acta Crystallogr., Sect. A: Found. Adv.* **2015**, *71*, 3−8.
(80) Dolomanov, O. V.; Bourhis, L. J.; Gildea, R. J.; Howard, J. A. K.; Puschmann, H. OLEX2: a complete structure solution, refinement and analysis program. *J. Appl. Crystallogr.* **2009**, *42*, 339−341.
(81) Spek, A. PLATON SQUEEZE: a tool for the calculation of the disordered solvent contribution to the calculated structure factors. *Acta Crystallogr., Sect. C: Struct. Chem.* **2015**, *71*, 9−18.

https://doi.org/10.1021/acs.organomet.1c00223
Organometallics 2021, 40, 1889−1906